THE C-E CECOR FIXED IN-CORE DETECTOR ANALYSIS SYSTEM

W. B. TERNEY
J. L. BIFFER
C. O. DECHAND
A. JONSSON
R. M. VERSLUIS

Nuclear Power Systems
Combustion Engineering, Inc.
Windsor, Connecticut

Presented at

AMERICAN NUCLEAR SOCIETY
ANNUAL SUMMER MEETING

June 12-17, 1983
Detroit, Michigan

CE POWER SYSTEMS

THE C-E CECOR FIXED IN-CORE DETECTOR ANALYSIS SYSTEM

I. INTRODUCTION

The Combustion Engineering (C-E) CECOR System provides a method of synthesizing detailed three dimensional assembly and peak pin power distributions from the signals of a limited number of fixed, self-powered neutron sensitive in-core detectors. The actual synthesis is done in the CECOR program using libraries of precalculated coefficients generated by the standard C-E diffusion and transport methods and codes. The system is used to fulfill the required startup testing, monitoring and surveillance functions as well as to provide the base of measurement information for core-follow and methods verification.

The fixed in-core detectors consist of self-powered rhodium neutron detectors. Each detector segment is 40 cm long and either four or five segments are equally spaced axially in each instrumented assembly. Approximately 25% of the assemblies are instrumented. A description of the instrumentation hardware is given in the following section, together with information on the reliability and reproducibility of the measured data.

The synthesis of signals into full-core three dimensional power distributions is carried out by the off-line CECOR computer program. CECOR has evolved from the earlier INCA program[1-5]. CECOR calculates the assembly power in each instrumented fuel assembly through the use of prefit power-to-signal assembly conversion factors (W'). The W' are provided for all instrumented assemblies in the core. They are obtained from fine mesh, multi-group diffusion theory calculations, with appropriate transport theory corrections. Full-core planar power distributions at each detector level are obtained through the use of precalculated average coupling coefficients, $< cc >$, which are the inverse ratio of the power in an uninstrumented assembly to the average power in its neighboring assemblies. The coupling coefficients are obtained from two or three-dimensional diffusion theory calculations. The resulting set of equations is solved for the power in uninstrumented assemblies. Axial power distributions are obtained by a few-mode Fourier expansion which matches the assembly powers at each detector level and uses axial boundary conditions derived from 3-D coarse mesh calculations. Subsequently, peak pin-powers in each assembly as a function of height are obtained by multiplying the assembly power at each height by assembly normalized local peaking factors, (F_p). These pin-to-box factors are obtained from fine-mesh, diffusion theory calculations with the appropriate transport theory corrections. The CECOR algorithms and required library are described in detail in Section III.

The accuracy of the system has been evaluated by combining the uncertainty in measured power for instrumented locations obtained from a large data base with the synthesis uncertainty for extrapolation to uninstrumented portions of the core.[6] This analysis is also described in Section III. The overall uncertainty for the CECOR system, which has been approved for C-E licensing submittals, has been quantified on the basis that there is a 95% probability that at least 95% of the true F_q, F_{xy}, and F_r values will be less than the values obtained from CECOR plus 6.2, 5.3 and 6.0%, respectively.

A basic function of the fixed in-core system is to satisfy monitoring and surveillance requirements. Through CECOR, it regularly provides both full-core, 3-dimensional power distributions and the limiting values of peak F_r, F_{xy}, F_q, as well as evaluations of the core tilt and axial shape indices. On current C-E plants it is also used to verify the operation of the COLSS and CPC limit monitoring and protection systems.[7] In addition, the system is used to produce measured power distributions for comparison with calculated power distributions calculated in core-follow analyses. Core follow analyses are performed as a customer service to determine if the core is operating as expected, and if not, to provide key diagnostic input to determining the causes of the difference. Measured power distributions are also used to validate methods and quantify calculation and measurement uncertainties. These various applications are discussed further in Section IV.

II. SYSTEM HARDWARE DESCRIPTION AND OPERATIONAL EXPERIENCE

A. Hardware Description

The fixed in-core instrument system hardware includes the instrument assemblies, guide paths and other supporting structures, field cabling and connectors, and signal conditioning and processing equipment. An overview is shown in Figure 1 for C-E's bottom-mounted, fixed plus moveable instrumented system, which is part of the 3800 MWt System 80. Figure 2 shows the axial position of the five detectors in a System 80 instrument assembly relative to the active core as well as the locations of the instrumented fuel assemblies in the core. Approximately 25% of the assemblies are instrumented. Each instrument assembly is inserted in a guide tube at the center of the fuel assembly. The bottom-mounted system permits instrumentation of both rodded and unrodded fuel assemblies. Earlier plants have a top-mounted design.

The C-E fixed incore instrumentation system employs the so-called self-powered neutron detector (SPNDS) with rhodium emitters 40 cm long and 0.045 cm in diameter. Each detector is an integral segment of a piece of coaxial, mineral insulated cable having an In-conel sheath and a 0.16 cm diameter central conductor. A string of 4 or 5 SPNDs is contained in an instrument assembly, which mechanically protects the detectors by means of an outer sheath, and positions them accurately. The assembly terminates electrically in a multi-pin electrical connector, which mates with the field cable connector. Mechanically it terminates in a seal plug which brings out the electrical leads through the primary pressure boundary. This is shown in Figure 3 for C-E's bottom-mounted system. Also shown is the calibration tube. It is a dry thimble which provides access for a movable detector in the combined fixed/movable in-core detector systems supplied on C-E's 3400 and 3800 MWt NSSS designs. Individual detectors are wrapped around the calibration tube within the outer sheath.

Rhodium-103 is the neutron-sensitive nuclide. It is mostly a thermal-neutron detector (it has a thermal-neutron cross section of about 100 barns) with an epither-

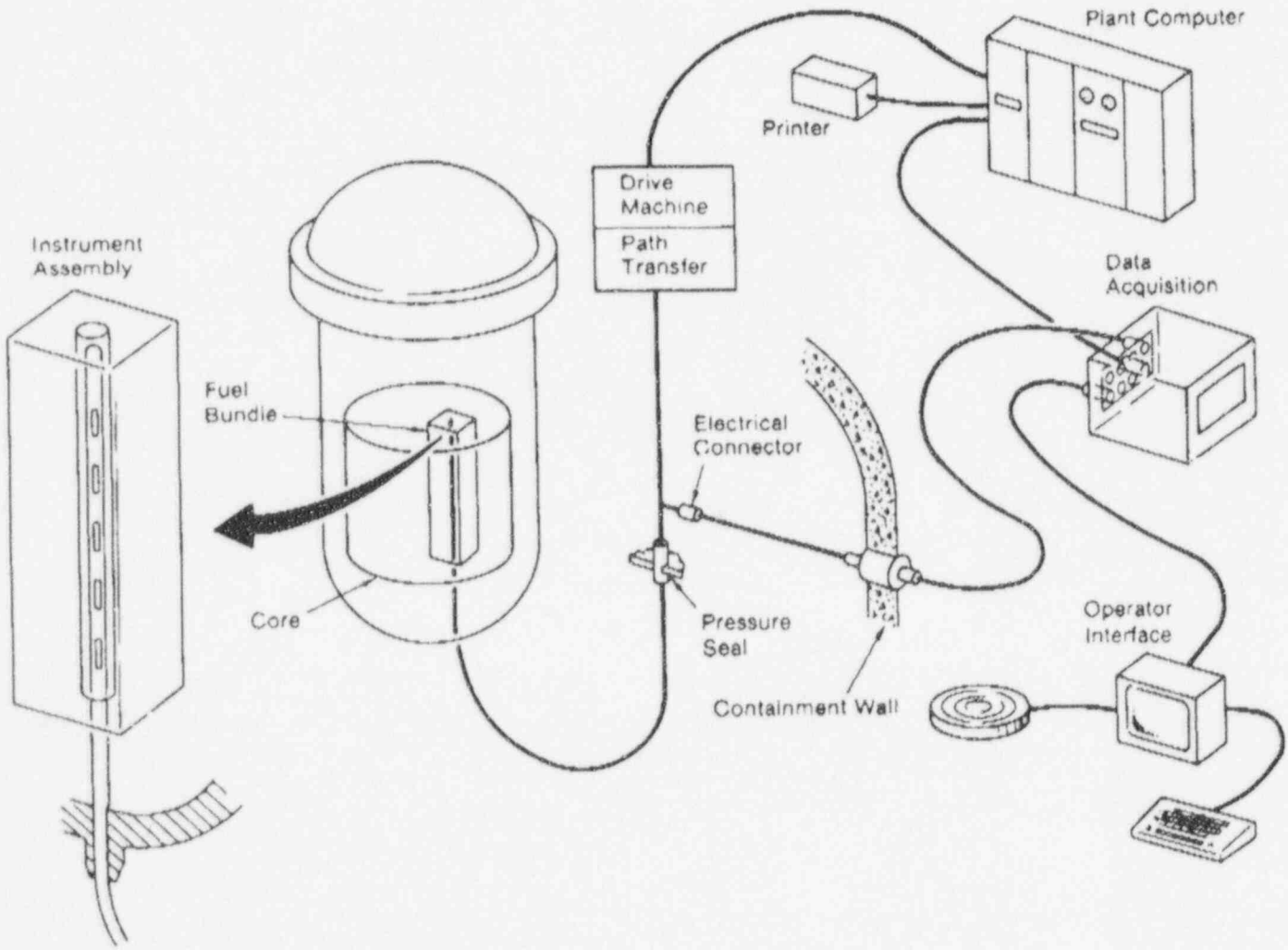

Fig. 1: Overview of fixed/moveable in-core instrument system

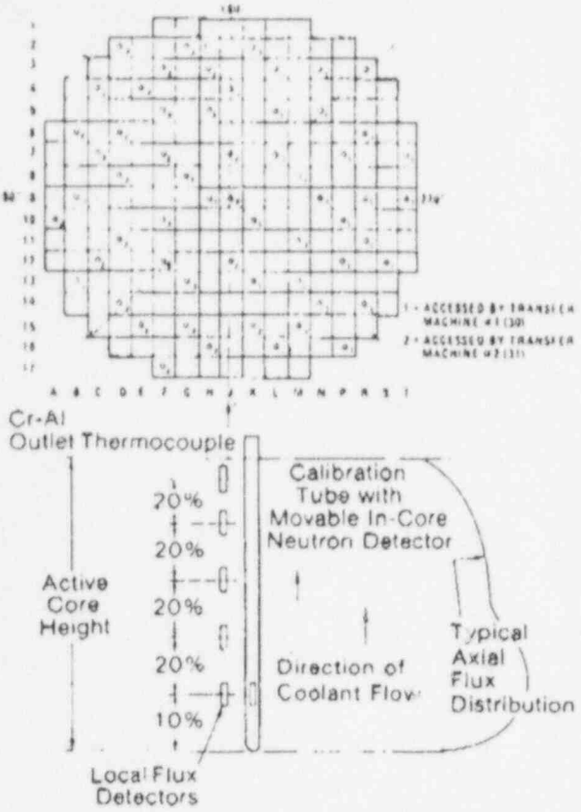

Fig. 2. System 80 fixed in-core instrumentation locations

mal contribution of about 15%. After absorbing a neutron, the rhodium-104 nucleus decays, emitting gamma and beta radiation. A fraction of the energetic betas (electrons) escape the emitter and are collected in the detector sheath, thus creating an "electron pump". If the circuit between the lead-wire and the sheath is closed, a current which is proportional to the neutron absorption rate is measured by the data acquisition system. About 6% of the betas are emitted promptly after neutron absorption; the remainder decays with a half-life of 42 seconds. For applications requiring a prompt response, C-E has constructed a dynamic compensation filter (Reference 8).

The small electrical current (about 2 micro-amps at nominal conditions) is conducted through well-shielded cable to the plant computer data acquisition system. Specially designed, low-impedance, high-gain current-to-voltage amplifiers, which also perform noise filtering, produce a 0-10 Volt output. This is multiplexed, and converted from an analog to digital signal. The signal is then further processed in the plant computer to correct for background, emitter burnup effects, and if needed, dynamically compensated for beta-decay effects.

Further processing consists of signal-to-power conversion, power distribution synthesis, and calculation of margins to core operating limits. These calculations are performed partially on the plant computer, on-line, and partially off-line in CECOR, with the split depending on NSSS vintage.

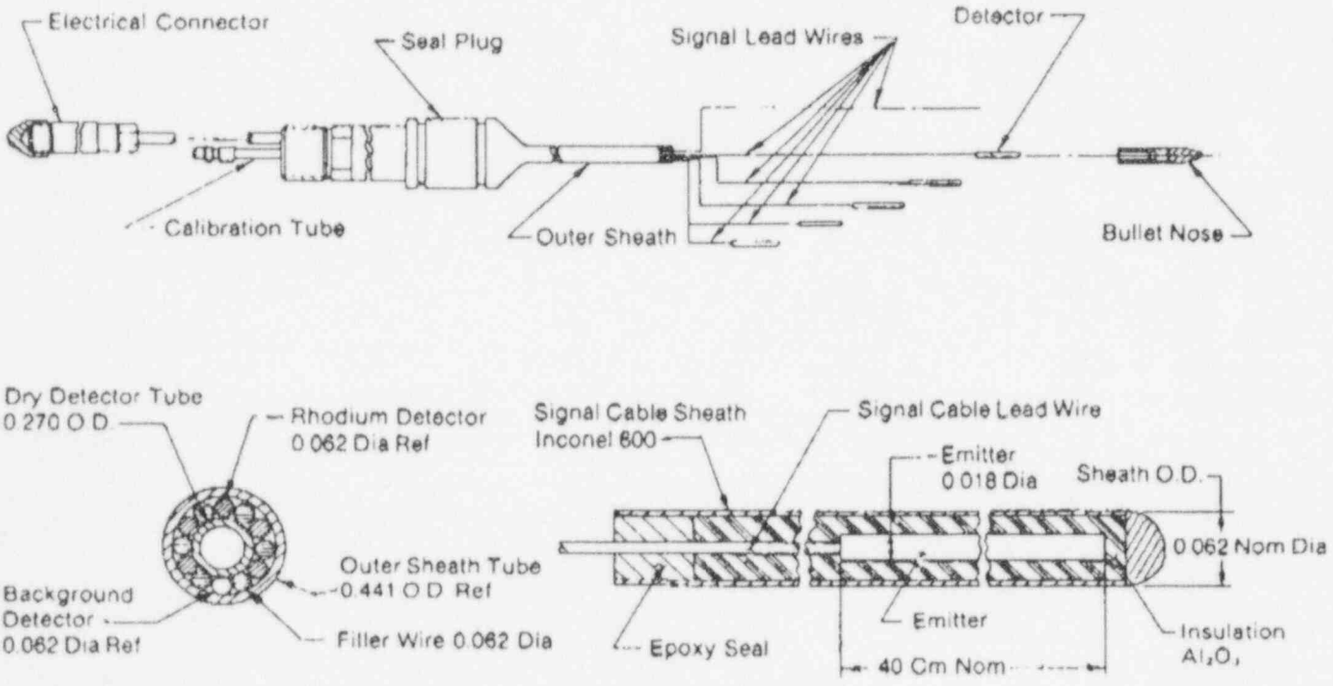

Fig. 3: In-core detector assembly

The mechanical layout of the instrument system and its support structure is shown in Figure 4 for C-E's bottom-mounted system. During refueling, while the water is at the vessel flange, the entire support frame including the moveable detector drive and transfer machinery is moved out of the way, after disconnecting the dry thimbles. This allows access to the seal table to dismantle the seals and withdraw the instrument assemblies by about 25 feet so the connectors and thimbles may be kept dry when the water level is raised to near the operating floor. This wet seal table arrangement during refueling permits the removal and disposal of instrument assemblies under water.

B. Operational Experience

In terms of its most important performance parameters, accuracy and availability, the C-E fixed in-core instrument system has an excellent record. By analyzing a sizable data base of measured power distributions, C-E has licensed the following 95/95 uncertainties[6]:

F_q	6.2%
F_r or $F_{\Delta H}$	6.0%
F_{xy}	5.3%

This analysis is described in more detail in Section III.C. As for availability, the in-core detector system has not limited core power performance in any plant. When judging this availability performance, it must be borne in mind that in C-E reactors, fixed incores not only fulfill the power distribution surveillance function, but also monitor the kw/ft limit and in doing so, provide considerably more margin to the LOCA limit than an ex-core monitoring system could obtain.

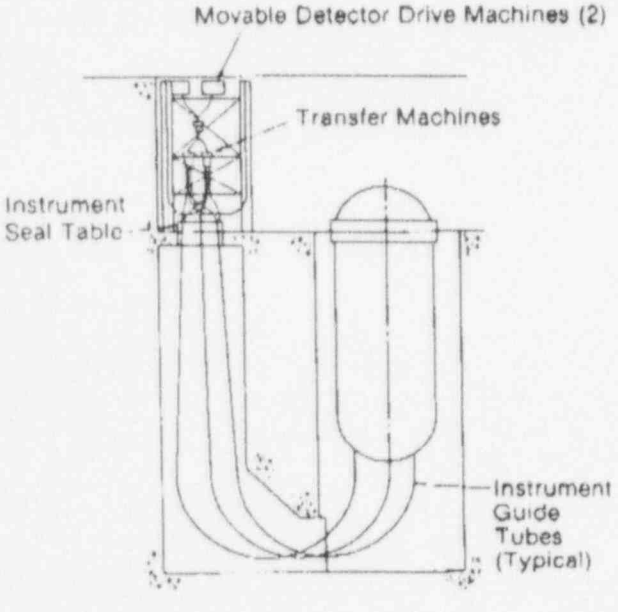

Fig. 4. Mechanical layout of instrument system

C-E's experience with the system spans 34 cycles of operation to date. Some of the early experience is found in Reference (9). As is to be expected, a number of design and manufacturing improvements were made to benefit from operating experience. The primary causes of detector failure are breaks in the lead wire and loss of electrical resistance between lead wire and sheath due to moisture.

Since the detector assemblies must be inserted and removed through tightly curved guide paths in the top-mounted systems employed in the pre-ANO-2 plants, they must be flexible and yet strong. This has resulted in a design for these plants with a permeable, flexible outer sheath and an extra internal member to increase tensile strength. This design has overcome earlier problems of breaking instrument assemblies during removal.

Because the sheath is permeable, the individual detectors are in contact with the coolant, which increases the chances of moisture ingress through corrosion. While moisture ingress still can occur, it has been greatly reduced by removing any welds, brazes or splices from the detector external surface ("integral" detector) and careful materials management and QA by the vendor.

Starting with Arkansas Nuclear One Unit 2 (ANO-2), all top-mounted in-core systems have combination fixed-moveable in-core detector assemblies and less complex guide paths. The solid sheath instrument assembly which is less flexible than the permeable sheath instrument assembly design has shown good performance in three cycles of operation at ANO-2.

Another improvement initiated in ANO-2 is to accomplish the current-to-voltage conversion required for signal multiplexing by active amplifiers, rather than dropping resistors. Dropping resistors are simple devices and free from drift, but they offer a high terminating impedance to the detector. Amplifiers offer significantly lower impedance, thereby reducing leakage currents that may occur in older detectors, and better noise filtering capabilities.

III. DESCRIPTION OF CECOR ANALYTICAL METHODS

A. Introduction

A description of C-E's original in-core detector signal analysis system, INCA, was published in 1969.[1] Since then, many improvements have been made and the code has evolved to the present CECOR system[2-5]. It provides a method to synthesize a limited number of fixed, self-powered, in-core detector readings into detailed full-core radial and axial distributions for assembly and peak pin powers.

Basically, CECOR uses prefit data from detailed, two-dimensional, multi-group diffusion theory calculations to convert detector readings to local box-power values through the use of power-to-signal (W') factors. These are provided for all instrumented assemblies in the core.

The planar power distributions at each detector level are obtained through the use of pre-calculated average coupling coefficients, < cc >, which relate the power in an uninstrumented assembly to the average power in its neighboring assemblies. The axial power distributions are obtained by a few mode Fourier expansion which matches the box powers at each detector level. Subsequently, the peak pin powers in each assembly are obtained by the application of pin-to-box (F_p) factors which are pre-calculated using fine mesh, two-dimensional transport-theory corrected diffusion theory.

The first section of this chapter describes the analytical methods in detail, starting with the conversion of signal to power, followed by a discussion of the types of edited output quantities. The second section of the chapter discusses the content and construction of the CECOR library. The final section describes the analysis used to quantify the accuracy of the system.

B. CECOR Algorithms

1. Signal-to-Box-Power Conversion

The power integral P_{in} over a detector level (n) in an instrumented assembly (i) is obtained by multiplying the background corrected, integrated detector signal (I^{Rh}_{in}) by constants measured and supplied by the vendor, and constants calculated from fine-mesh, two-dimensional, multi-group diffusion theory calculations. The signal-to-box power conversion for an instrumented assembly i at detector level n is expressed by:

$$P_{in} = I^{Rh}_{in} W_{in} \tag{1}$$

where

$$W_{in} = \frac{CALIB \cdot W'_{in}}{S^{Rh}_{in}} \tag{2}$$

$$W'_{in} = P_{in} / \int_E \int_{V_{in}} \sigma^{Rh}_a (N^{Rh}) \phi(\underline{r},E) d\underline{r}\, dE \tag{3}$$

and where CALIB is a factor to convert from surface flux to Rhodium activation and the double integral represents the Rhodium activation in the detector.

The initial detector sensitivity, S_o, relates the current, I, produced by the detector to the incident neutron flux at the surface of the detector. The initial sensitivity and relative calibration of the sensitivity are supplied by the vendor. The sensitivity as a function of depletion for a given detector is determined by

$$S^{Rh}(t) = S_o \left(1 - \frac{Q(t)}{Q_\infty}\right)^n \tag{4}$$

where

- Q = accumulated charge
- S_o = the initial sensitivity for the detector, supplied by the vendor.
- $\frac{Q(t)}{Q_\infty}$ = the fraction of the total available charge for the detector at time t, where Q_∞ is supplied by the vendor.
- n = the empirically determined fitting parameter.

The W' are calculated for each assembly with a detector as a function of life from transport corrected fine-mesh, 2-D planar depletion calculations using multi-group diffusion theory. The W' are then fit as a function of assembly burnup for each detector location and take into account whether an assembly is rodded or not. The behavior of W' with burnup is illustrated in Figure 5 for typical assemblies in the different batches of a first cycle core.

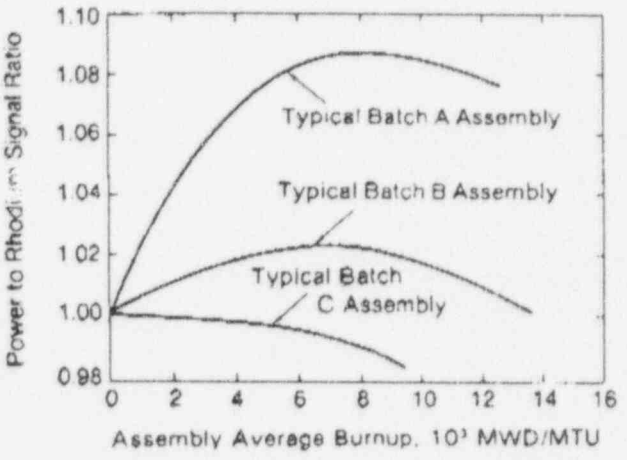

Fig. 5: Power to rhodium signal conversion factors vs assembly average burnup

2. Planar Power Distributions

At each detector level the powers in the uninstrumented assemblies are determined from the measured powers in instrumented assemblies. This is accomplished through the use of radial coupling coefficients.

The average coupling coefficient of an assembly at detector level n is defined as the ratio of the average power in the surrounding boxes to the power in the assembly itself. For the case of a cell surrounded by N_j boxes, this is

$$\langle cc \rangle_{in} = \frac{\sum_{j=1}^{N_j} P^i_{jn}}{N_j P_{in}} \tag{5}$$

where P^i_{jn} denotes the power in boxes neighboring cell i.

The average coupling coefficient given by Eq. (5) is insensitive to mild power tilts across the core. In addition it has been found that local perturbation effects in a cell (e.g., from rods) essentially affect the coupling coefficient for only the subject box; i.e.,

$$\delta\langle cc\rangle_{in} = \frac{-h'}{N_i M_{in}^2}\,\delta k_{\infty_{in}} \qquad (6)$$

as can be derived from the modified one-group diffusion equation.[5] Eq. (6) has, in fact, been tested and found to accurately predict such perturbations in $\langle cc\rangle_{in}$.

In practice, the coefficients are pre-calculated from Eq. (5) using box power distributions obtained from either 2-D fine-mesh or 3-D coarse-mesh depletion calculations using multi-group diffusion theory, and are then fit as a function of burnup for each assembly. Explicit sets of burnup-fitted coefficients are prepared for each control rod configuration or rod bank region. The actual values of $\langle cc\rangle_{in}$ used in CECOR are obtained from these sets of fitted coefficients using average assembly burnup values obtained by integration over detector level n. A typical example for an assembly in a rodded and unrodded condition is shown in Figure 6.

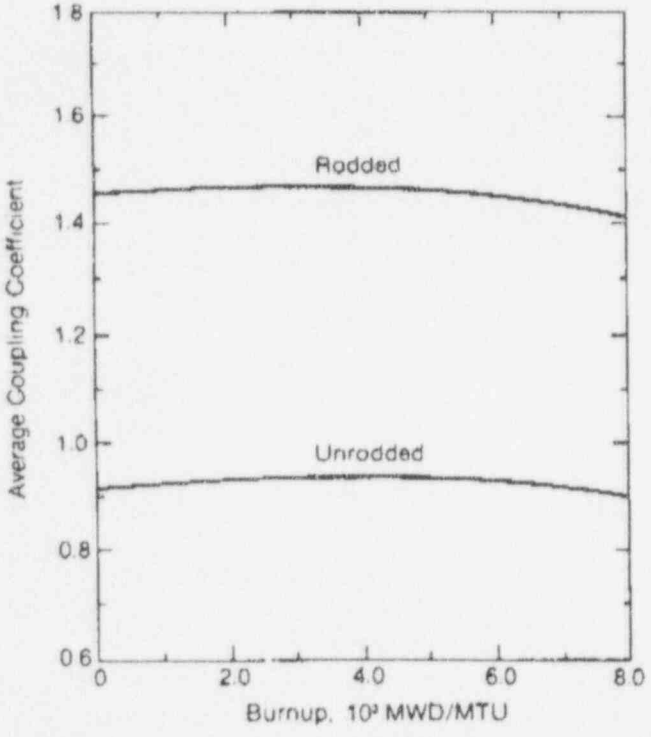

Fig. 6: Typical average coupling coefficient behavior

Knowing the average coupling coefficient values at a given detector level, the power in any uninstrumented box ℓ may be obtained from:

$$P_{\ell n} = \frac{\sum_{j=1}^{N_\ell} P_{jn}^{\ell}}{N_\ell \langle cc\rangle_{\ell n}} \qquad (7)$$

Originally[1], INCA worked on an octant or quarter core basis, where symmetry was assumed and all instrument readings were reflected into the octant of interest. As a consequence, each uninstrumented box was surrounded by four instrumented boxes and Eq. (7) itself could be solved directly for each uninstrumented box. In the actual CECOR full core calculation, each uninstrumented box is not surrounded by four instrumented neighbors. In fact, many boxes have only one or two instrumented neighbors; and some have none. As a result, Eq. (7) cannot be solved directly for each uninstrumented box alone, since some of the neighboring powers are also unknown. However, at each level n, the equation may be written for every uninstrumented box, and then rearranged with the unknown powers on one side of the equation and the known powers on the other. When all the equations for each uninstrumented box are written and grouped, a matrix equation results:

$$A\,\underline{P} = \underline{S} \qquad (8)$$

The A matrix is symmetric and very sparse. In each row the diagonal element is the product of the number of neighbors times the coupling coefficient. The off-diagonal elements are all zero except for the 3-4 positions of the uninstrumented neighbors of the assembly, when the value is -1. If uninstrumented assemblies are surrounded by four instrumented assemblies, this new CECOR formulation reverts back to the original INCA scheme.

The solution for the unknown powers is obtained by solving Eq. (8). Symbolically:

$$\underline{P} = A^{-1}\,\underline{S} \qquad (9)$$

This system is solved at each detector level.

Since the matrix can be large (on the order of 200x200), efficient solution routines are needed. Because of speed and memory requirements, a modification of the conjugate gradient method[10] which takes advantage of the unique nature of the A matrix is used.

A feature of this formulation is that if an instrument fails, the box is simply treated as uninstrumented and the resulting larger set of equations is solved. For this to work, average coupling coefficients are precalculated and provided for all boxes, uninstrumented or instrumented.

This concept also provides a way of checking detectors, since the actual detector power may be compared to the deduced power obtained by treating the box as uninstrumented. If the difference exceeds a predetermined criterion, it is an indication that either the detector has failed or a local perturbation may have occurred.

3. Axial Power Distribution

Using the power in the assembly at each detector level, the detailed axial shape can be synthesized by using a Fourier expansion. This axial fitting technique is described in detail in Reference 3. Basically, the axial power distribution in an assembly is represented as the sum of the first N Fourier modes

$$P_i(z) = \sum_{n=1}^{N} a_n \sin n\pi B_i z \qquad (10)$$

where $P_i(z)$ is the power per unit length for assembly i, a_n are the unknown combining coefficients, z is the axial elevation in fraction of the core height, H, and B_i is the fitting parameter given by

$$B_i = \frac{H}{H + 2d_i} \qquad (11)$$

Note that d_i is essentially an extrapolation distance. The N combining coefficients, and thus the axial power distributions are obtained by matching the box power at each level to the integral of Eq. (10) over the axial extent of each of the N detectors. Thus,

$$P_{in} = \int_{\beta_n}^{\alpha_n} dz \left(\sum_{n=1}^{N} a_n \sin n\pi B_i z \right), \quad n = 1,\ldots,N \qquad (12)$$

is used to solve for the a_n values for assembly i, where β_n and α_n are the elevations for the bottom and top of detector level n, respectively. For instrumented assemblies, the P_{in} values are obtained directly from detector measurements. For uninstrumented assemblies, the values are obtained from planar power distribution solutions at each level, using the coupling coefficient formulation described in III.A.2. For all C-E cores, an n-mode Fourier expansion is used to match all n detector powers simultaneously, where n is either 4 or 5.

An important parameter in the Fourier expansion is the extrapolation distance (d) or fitting parameter B. It is a function of core life and is radial core zone dependent. B is obtained from nominal 3-D design depletion studies. It is chosen for each zone so as to minimize the error in fitting the axial peak to average power ratio in each assembly. It is a well-behaved function of burnup, as illustrated in Figure 7.

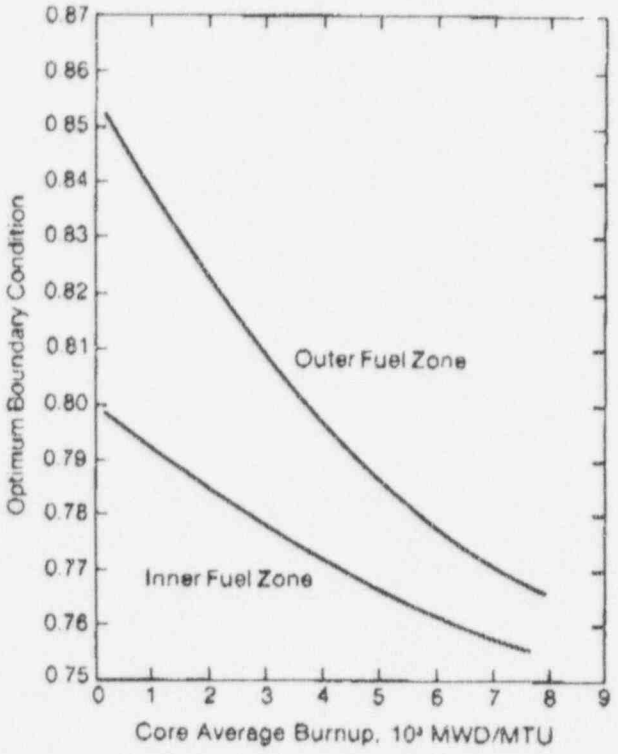

Fig. 7: Typical cycle 2 CECOR axial boundary conditions

4. Total Power, Pin Peaks, and Alarm Limit Ratios

Determination of radial and axial power distributions for the assemblies is completed using the methodology described in the previous sections. The core power is normalized to the calorimetric power. The nodal burnups are updated by integrating the energy production over the elapsed time since the previous time point. This information is used to update the assembly, batch, and core exposure counters. These, in turn, provide information advantageous to fuel management, and are used to evaluate the fits for CECOR coefficients.

Detailed three-dimensional peak pin power distributions are obtained axially at each node for each assembly through the use of precalculated pin to box (F_p) factors,

which are fit to the assembly burnup. The pin to box factor is defined as the ratio of the maximum 1-pin power in the box to the average pin power in the box. The precalculated values are obtained from detailed two-dimensional depletion calculations, using multi-group, transport theory corrected diffusion theory, for each rod bank configuration or region. Typical examples of the burnup behavior of F_p for different assemblies are given in Figure 8. The peak pin power at any axial location is then obtained using

$$P_i(z) = F_{pi}(z)\, P_i(z) \qquad (13)$$

where $F_{pi}(z)$ is taken from the appropriate coefficient set and evaluated with the local assembly burnup at that elevation.

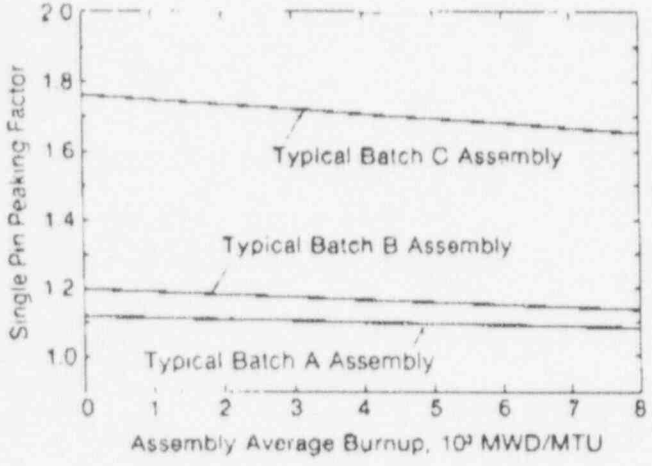

Fig. 8. Single pin peaking factor variation with burnup

The 3-D pin power distributions can then be examined to find the peak pin power (F_q) for each assembly and for the core (F_q). Axial integrals can be formed to find the peak pin channel power (F_r) for each assembly and for the core (F_r). Further, the peak pin power to the average pin power can be obtained for each axial elevation, $F_{xy}(z)$, and for the core as a whole, (F_{xy}). Conversions are also made to give peak linear heat rates in terms of actual powers rather than as ratios, and also as alarm limit ratios. The code also provides most of the parameters required to estimate DNB ratios. The DNBR calculation is not performed in CECOR, but through the link to peripheral codes.

C. CECOR Libraries

1. Formalism

The INCA/CECOR system relies on the use of a large library of predetermined coefficients which are used to convert the measured signals into detailed, three-dimensional assembly and peak pin power distributions. The values of these coefficients depend on the assembly and axial location, core configuration, and the local assembly or nodal burnup.

The library coefficients <CC>, W', and F_p defined above are currently obtained from detailed, two-dimensional depletion calculations[11] using multi-group diffusion theory. Each assembly, instrument, and pin cell is explicitly represented in these calculations for each normal control rod configuration. The coefficient values are calculated for each assembly and instrument, and are fit as functions of the local burnup for each assembly. The two-dimensional calculations are taken to represent explicit axial regions or planes in the core.

For first cycles, which generally have separable power distributions, a core average plane is used with the various control rod configurations for cores with either four or five detector levels. For later cycles, which generally do not have separable power distributions, a plane representing the axial mid-region of the core is currently used. This leads to acceptable uncertainties, on the order of 5-6%, as shown in Reference 6. However, the use of several different planes to represent the different axial regions of the core would lead to lower uncertainties, since the axial variation of the coefficients would be included. The transition to multi-level coefficients obtained directly from the normal, reload 3-D calculations is underway for reload cores with either four or five detector levels. This will lead to lower synthesis uncertainties than those quoted in Reference 6, and will remove conservatism as is shown in Section IV.

2. Generation and Quality Assurance of CECOR Libraries

It is apparent from the previous sections that the CECOR libraries are both large and complex. In a typical application, approximately 5000 coefficients must be stored and retrieved upon demand. An automated computer code system has been developed to facilitate both the generation and quality assurance of these libraries. The sequence of steps required to produce a typical library is shown schematically in Figure 9.

The generation of the basic data required for CECOR, i.e., the pointwise powers, fluxes, and concentrations, is currently performed through standard fine mesh diffusion theory calculations using the PDQ-7 computer code.[11] Approximately 15 such calculations are required. Primary editing of the PDQ-7 files is performed by the CERISE code. This operation transforms the pointwise PDQ-7 data into assembly-wise data required by CECOR. Summary files are written for use in Paths

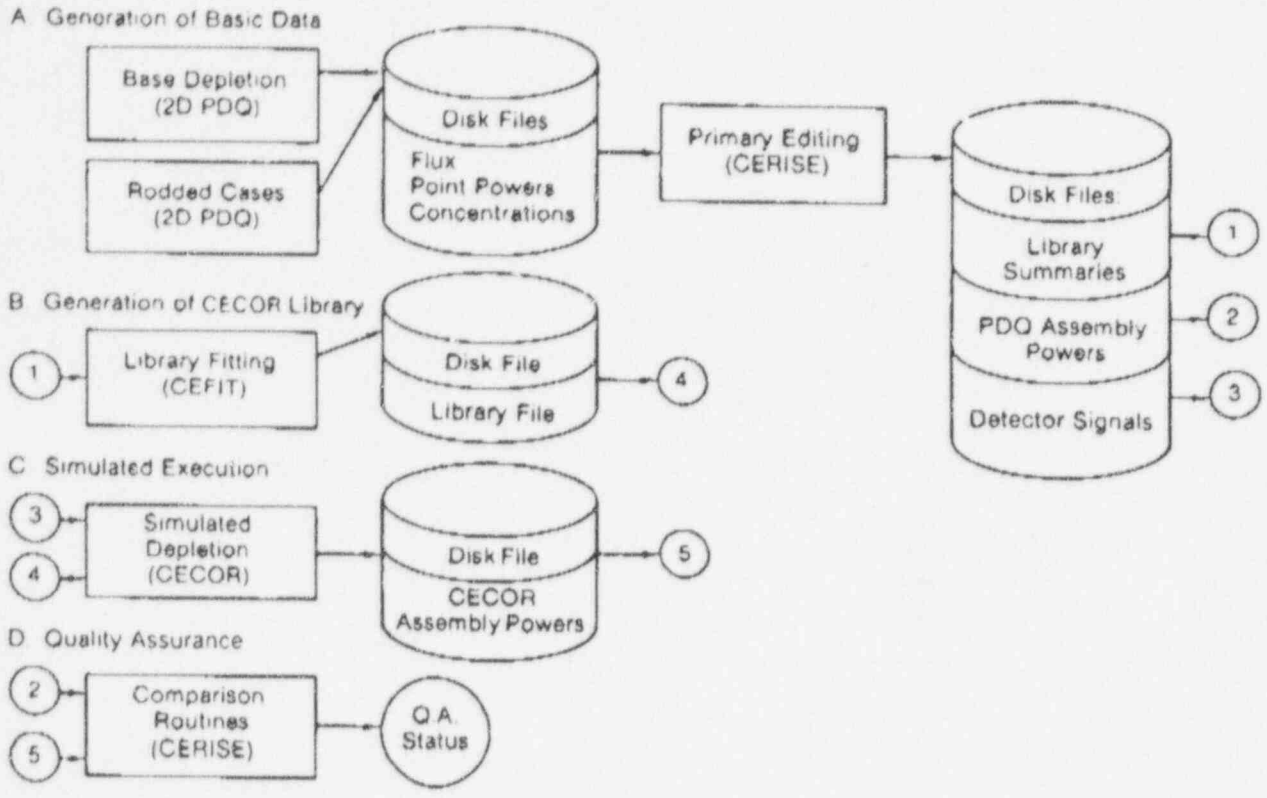

Fig. 9: Generation and quality assurance of CECOR libraries

B-D in Figure 9. Detector signals consistent with the library are also generated for testing the completed library.

The generation of the CECOR library is indicated in Path B of Figure 9 and is the work of the CEFIT code. At this stage libraries are available for either quality assurance testing or actual use at the reactor site.

All the codes[11-16] used in generating the libraries and their functions are given in Table 1. These codes are quality assured and maintained in accordance with internal quality assurance procedures for computer codes. To adequately test the library, the CECOR code is executed using the file created in Step B and the signals in Step A in a fashion identical to the manner in which the PDQ-7 cases were executed. The results are stored and compared to the original CERISE data (Step D).

Final testing of the CECOR program and libraries must be performed at the reactor site. Sample test cases from the above effort serve to verify the coding and the data. Test results and procedures are properly recorded and documented for future reference.

D. Accuracy of the System

The error inherent in the use of the CECOR program can be broken into four components. These are: (1) basic box power measurement uncertainty due to the instruments, (2) box power synthesis uncertainty for the extrapolation to uninstrumented locations, (3) pin peaking synthesis uncertainty, and (4) pin peaking calculative uncertainty. These are then statistically combined to yield overall uncertainties. Details are provided in Reference 6.

The basic measurement uncertainty is the error associated with the measurement of assembly-average power in instrumented locations. It includes uncertainties in raw detector signal, background correction, initial calibrated detector sensitivity, sensitivity depletion, and signal to power conversion. The measurement uncertainty was evaluated by comparing the large data base of measured and calculated box powers with the calculational error removed. The uncertainties are evaluated for the local peak power to core average power ratio (F_Q), planar peak power to planar average power ratio (F_{xy}), and axially integrated peak power to core average power ratio (F_r).

An alternative formulation uses the powers in symmetric instrumented assemblies to provide an estimate of the F_Q, F_{xy}, and F_r basic measurement uncertainties. The advantages of this approach are that the uncertainty components are available at the same time as other CECOR results. Further the calculation does not require 3-D ROCS results for comparison purposes. The results of the two methods are essentially identical as shown in Table 2.

TABLE 1
SUMMARY OF COMPUTER CODES
USED IN GENERATION OF CECOR LIBRARIES

Code	Type	Description	Typical Number of Cases
DIT/CEPAK (14, 15, 16)	Cross section generation	standard design depletion calculations	5 depletions (of 10 time steps each)
PDQ-7 (11)	2-D fine mesh 2 or 4 group diffusion theory calculations	standard unrodded design 2-D depletion plus several rodded cases	15 cases
ROCS (12, 13)	3-D coarse mesh 2-group diffusion theory calculations	standard unrodded design 3-D depletion	10 cases
CERISE	PDQ-editor	provides edited information (i.e., detector signals, assembly power, etc.)	one for each PDQ-case
CEFIT	CECOR library generator	fits all CECOR coefficients to burnup and provides properly formatted library	one per core

TABLE 2
COMPARISON OF
CALCULATION-MEASUREMENT AND
SYMMETRIC INSTRUMENT STATISTICS RESULTS

Quantity	Core Follow Method	Sym. Inst. Method
Fxy	.0189	.0183
Fr	.0157	.0139
Fq	.0189	.0183

The box power synthesis uncertainty is the error associated with the radial and axial extrapolation of measured box powers to uninstrumented locations. These errors arise from radial coupling by means of the CECOR coefficient library and the Fourier expansion from 4 or 5 axial detector locations to all axial points. The uncertainty components for F_Q, F_{xy}, and F_r are obtained by comparing box powers from reference 3-D coarse mesh diffusion theory calculations (ROCS) to box powers from CECOR synthesis calculations using test signals derived from the reference 3-D depletions and single-level CECOR coefficients obtained from consistent 2-D planar depletions.

The pin peaking synthesis uncertainty is the error associated with the axial synthesis of maximum pin powers using CECOR pin-to-box coefficient libraries constructed from single-plane depletion calculations. It is evaluated by comparing pin-to-box factors from 2-D planar calculations representing a mid-plane and a top-plane.

The pin peaking calculative uncertainty is associated with the basic calculational error in the pin-to-box factor used in the CECOR synthesis, which is obtained from transport theory corrected diffusion calculations. It is evaluated by comparing calculated pin powers against pin powers from critical assemblies.

The components of these four uncertainties are then combined statistically to obtain overall uncertainties for F_Q, F_{xy}, and F_r. As shown in Reference 6, the overall CECOR uncertainty is such that there is a 95% probability that at least 95% of the true F_Q, F_{xy}, and F_r values will be less than the values inferred from CECOR measurements plus 6.2%, 5.3%, and 6.0%, respectively. This is summarized in Table 3.

IV. APPLICATIONS OF THE CECOR SYSTEM

CECOR is used in a number of applications, by both utility and C-E personnel. It is the source of operating data for routine monitoring and surveillance functions

TABLE 3
APPROVED CECOR UNCERTAINTY VALUES

Quantity	95/95 Uncertainty (%)
Fq	6.24
Fxy	5.29
Fr	6.04

and is used to verify the operation of the on-line COLSS monitoring and CPC programs[7] on newer C-E plants. It is especially important during startup test phases for new plants and new cycles. Normal core follow activities involve comparisons of predictions and CECOR measured data. On a few occasions, core follow activities have revealed core or plant computer problems. Also, design code and method verifications are made possible with the use of CECOR measured power distributions. This has led to improvements in codes and methods. A more recent activity has been the verification of the sensitivity depletion law given in Equation 4.

A. Core Monitoring and Surveillance

CECOR is used to provide operating plant data for comparison with limiting conditions of operation (LCOs) and for verification that the plant is operating within the Technical Specifications limits. Among the data recorded are the planar radial peaking factor (F_{xy}), integrated radial peaking factor (F_r), 3-D 1-pin peak (F_q), axial shape index, axial peak to average power azimuthal tilt magnitude, as well as radial and axial power distributions.

For the newer C-E plants, CECOR is used to verify the operation of the Core Operating Limit Supervisory System (COLSS) and the Core Protective Calculators (CPC).[7]

In addition to the normal surveillance functions, CECOR is used during plant and cycle startup tests to verify key core parameters.

B. Core Follow

Core follow activities encompass several of the CECOR functions. Monitoring data and detailed 3-D power distributions are recorded as a function of core lifetime to determine trends in important core parameters. In this way, the proper functioning of the core is verified. Figures 10 through 12 are examples of data trended in typical core follow efforts. These include the CECOR measured values and the values calculated by the ROCS design method. When the core is not operating as expected, the reason may be an actual core anomaly, site problems or design model deficiencies. Examples are discussed briefly in the following sections.

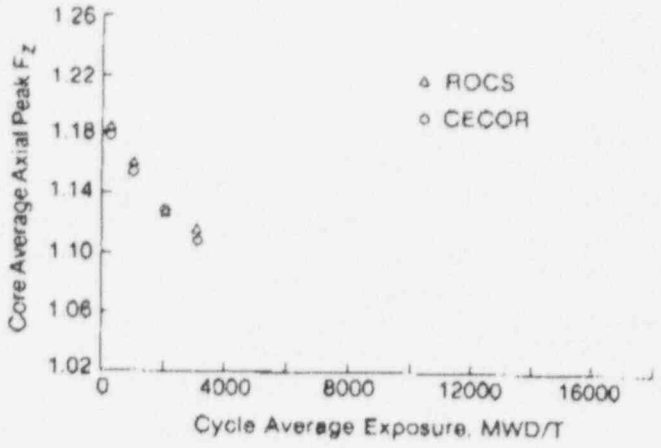

Fig. 10: ROCS and CECOR axial peaks (FZ)

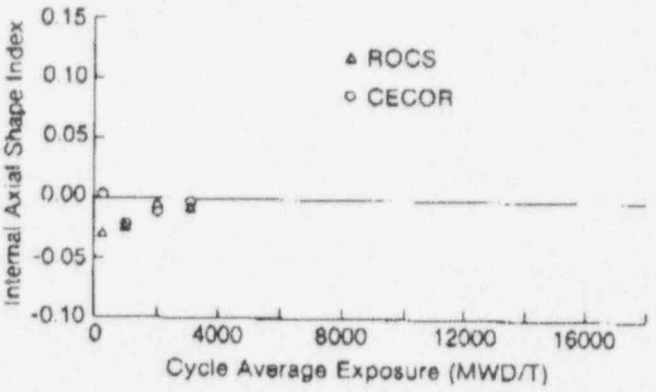

Fig. 11: ROCS and CECOR internal axial shape indices

C. Diagnostics

When basic core follow and instrument follow programs uncover disparities between measured and calculated data, it is necessary to determine the cause. Sometimes this reveals a core anomaly or some error in the analysis systems. The CECOR system has proved useful in this process as the following examples demonstrate.

In the past, core follow activities pointed out the possibility of shim failures in the first cycle of an early plant. This was discovered during core follow of the startup phase for the plant. There was a 20% increase in the measured core average axial peak within one month of startup, as shown in Figure 13, rather than the normal flattening of the distribution. Normal standard deviations for radial comparisons are in the range of 1% to 2%, versus the 4% seen in Figure 14. Also, an increasing reactivity error with burnup was noted indicating a loss of poison. Of the possible causes for this behavior, it was

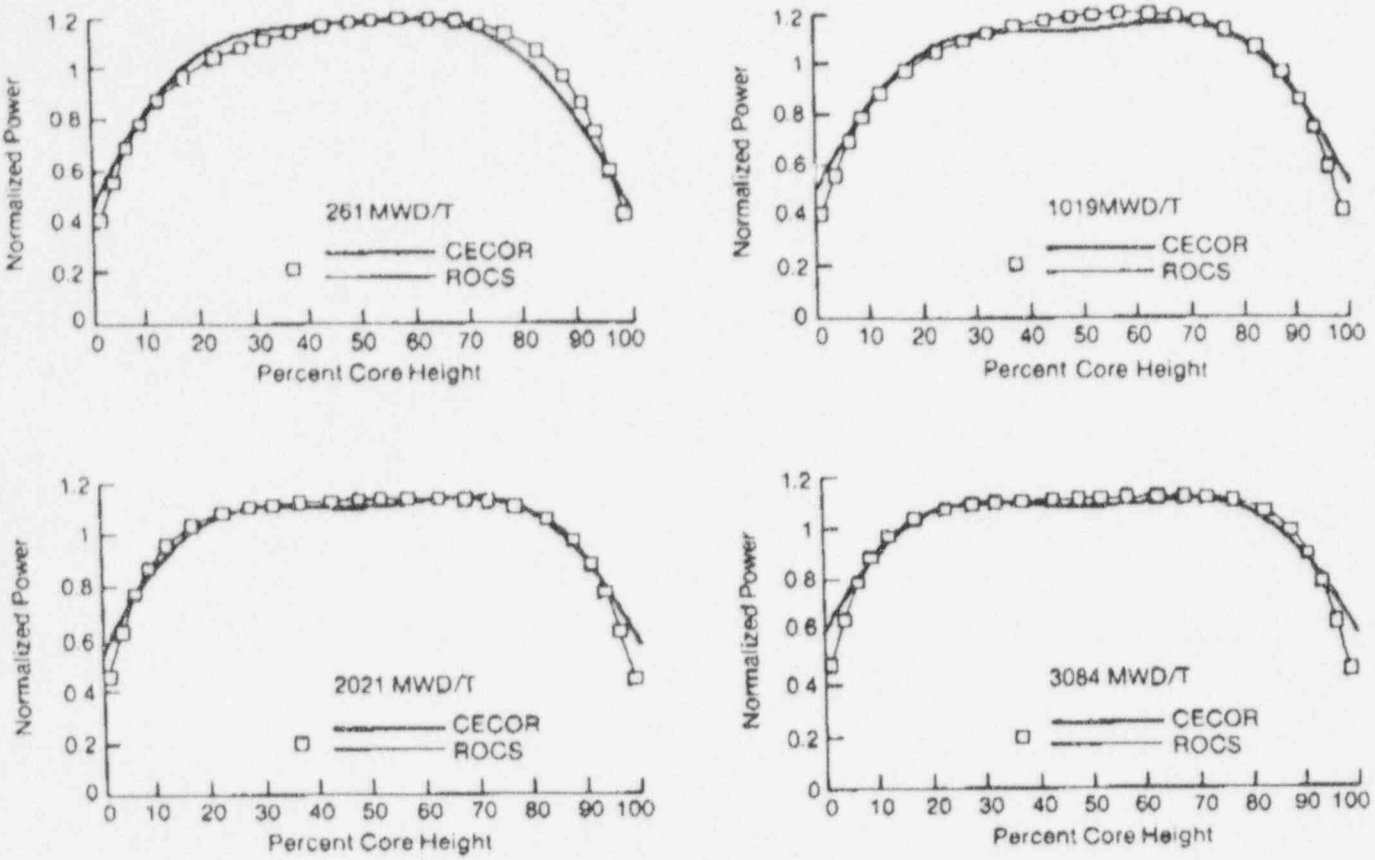

Fig. 12. Comparison of ROCS and CECOR axial power distribution

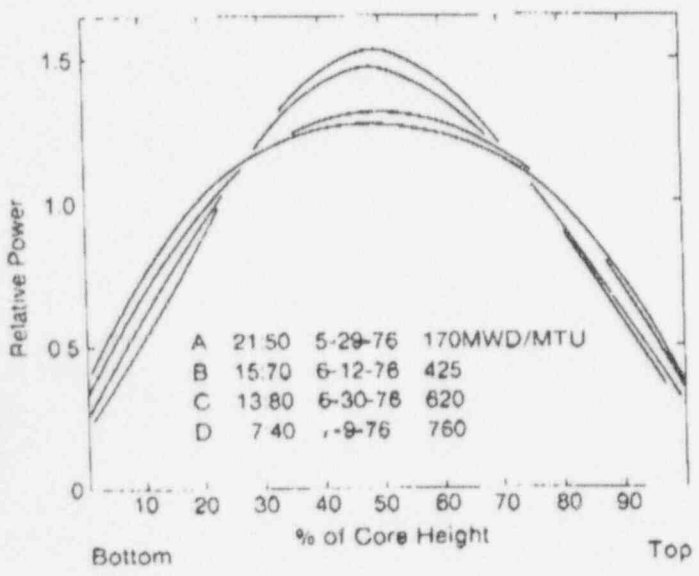

Fig. 13. Axial power shapes for four early snapshots showing effect of shim failure

concluded that some form of shim failure could explain the observed effects with the proper magnitudes. Subsequent studies of the removed shims confirmed this (Reference 17).

Crud deposits have occurred in a number of plants both in the U. S. and Europe. A recent case was detected by noting that measured power distributions were shifted in towards the core center and down towards the core bottom. This is thought to result from crud preferentially depositing in regions of elevated temperature in the core.

Figure 15 shows the ROCS and CECOR values for the core average axial shape index as a function of burnup. The largest discrepancy is near 3000 MWD/t, and the large measured positive value (.075) means the power moved to the core bottom. Figure 16 shows the calculated and measured values of the core average peak to average power, F_Z, as functions of burnup. The large difference between ROCS and CECOR indicated a problem with the core axial power distributions after the initial good agreement. This is confirmed by Figure 17, which shows core average axial power profiles for four time points in

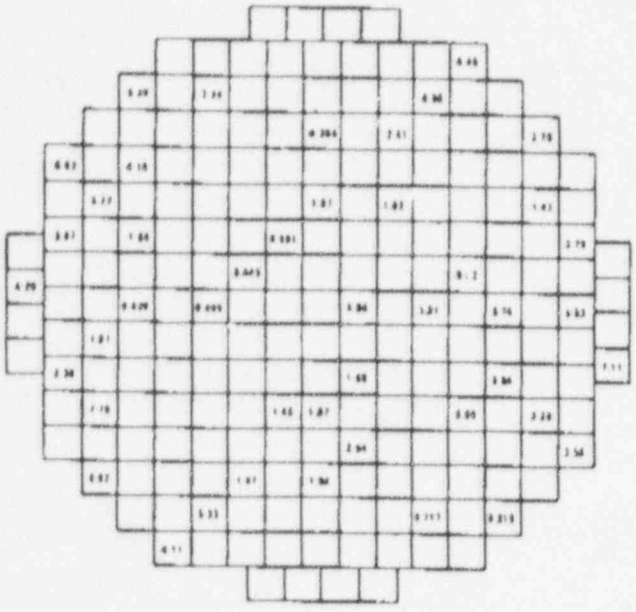

Standard Deviation of Differences 4.06%

Fig. 14: Relative power density in instrumented assemblies (percent difference between calculation and measurement) showing anomalous shim behavior

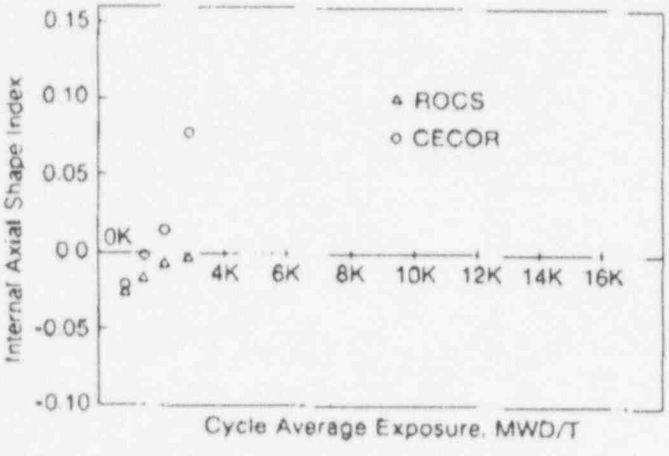

Fig. 15: Internal axial shape index (ASI) vs cycle average exposure showing effect of crud

the cycle. The shift to the core bottom by 2854 MWD/t is easily seen. This was accompanied by a radial power roll to the core center as shown in Figure 18 by comparisons of ROCS and CECOR powers at the four axial detector levels (20, 40, 60, and 80% of core height, respectively). Proceeding up the core from level 1 to level 4, a greater fraction of the level power is shifted into the core center. The formation of crud was attributed to air leakage into the makeup water systems; when this was corrected and the primary system treated, the power distribution returned to normal.

Of course, there need not be actual core problems to

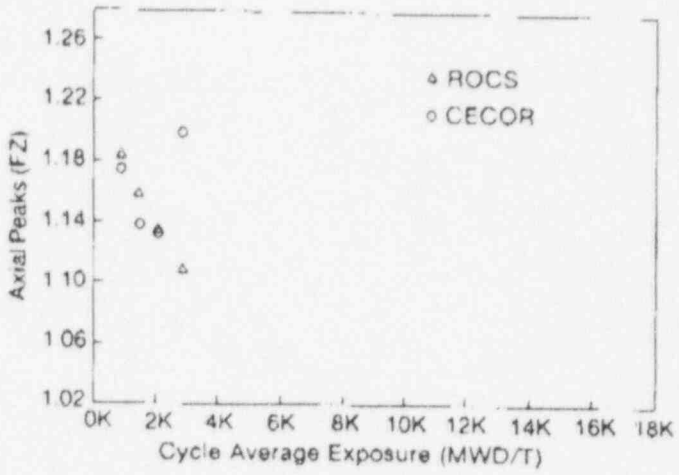

Fig. 16: Axial peaks (Fz) vs cycle average exposure showing effect of crud

affect the power distributions inferred from in-core instrument data. Recently, during a plant computer restart, excessive incore detector depletion was inadvertently entered. This was detected in the course of normal instrument-follow activity (Figure 19). The sensitivity is depleting linearly in a reasonable fashion, up through about 4500 MWD/T. The discontinuity in the lines occurred after a plant outage when the plant computer was updated to account for the computer outage. The downtime was mistakenly entered as 10 days instead of 1. Following the break in the lines, the depletion continues with the same proper slope as the original lines, but starting from the incorrect value. It was possible to locate the time of the problem to within the exact day, as seen in the figure.

During a later cycle of one of the five-detector plants, core follow comparisons of measured and calculated power distributions showed considerable disparity between instrumented and uninstrumented symmetric bundles. A clue to the nature of the problem was the detector-level dependent nature of the discrepancies. The problem was traced to the fact that a single level (midplane) set of CECOR radial coupling coefficients was being used to represent all axial levels of this taller, five-detector core. Thus, the substantially different burnup profiles and reactivity at the different levels in new and old fuel were not explicitly accounted for axially. Since the CECOR system of programs was explicitly designed to produce and utilize multi-level CECOR libraries, a 5-level coupling library was produced. When the level dependent library was used, the discrepancies disappeared. It is planned to use multi-level coefficients as a matter of course in future reloads.

An additional benefit of the multi-level approach is the reduction in over-conservatism for peak monitoring data. The use of single-level coefficients gives highly conservative values of peaking towards the top of the core. This is illustrated in Figure 20 which shows a comparison

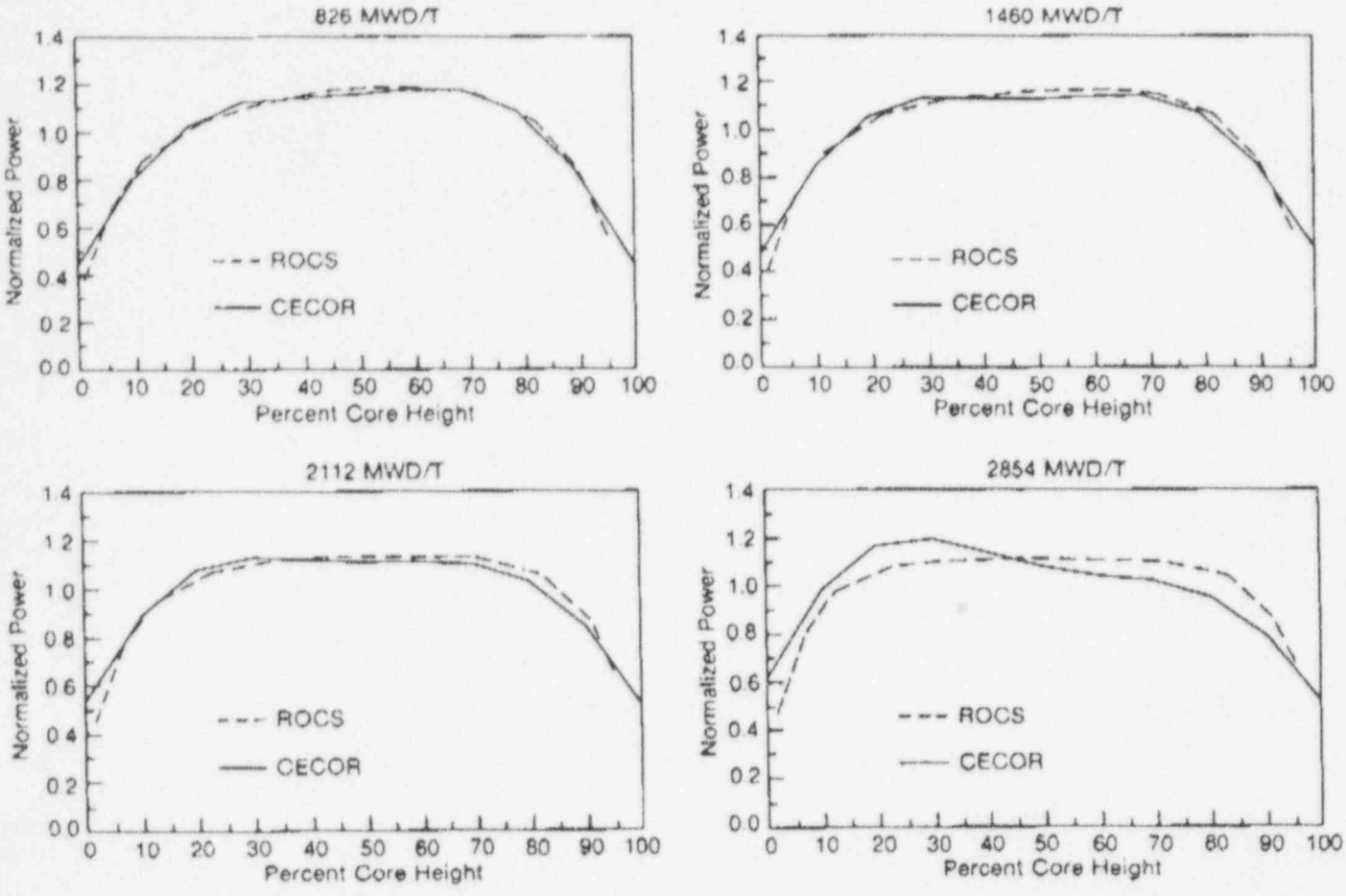

Fig. 17: Axial power distribution comparison showing effect of crud

of the assembly planar peaking factors from a 3-D ROCS calculation and a CECOR simulation. The CECOR simulation was run using single-level coefficients and signals from the 3-D ROCS. The use of multi-level coefficients removes this over-conservatism, as seen in Figures 21 and 22.

D. Verification of Design Codes and Methods

Over the years, many improvements have been made in C-E design codes and methods. These changes grew in response to benchmarking against both critical experiments and the ever-increasing data base of CECOR results from operating power reactors. A few of these resulting improvements are summarized here.

In the mid-1970's, comparison of measured and calculated CECOR (INCA) power distributions showed that 4 group diffusion theory models overpredicted power distributions in the center of the core by a few percent, and underpredicted the distributions at the core periphery by a similar amount. The problem was traced to the reflector treatment in diffusion theory calculations. Diffusion theory was underpredicting the albedos of the reflector regions in the fast group. An analytic study was carried out[18] which led to the derivation of a corrected fast diffusion constant which forced the agreement of diffusion theory and transport theory albedos. The work was extended for both 2 and 4 group and fine and course mesh diffusion theory calculations. The use of the formalism leads to good power distribution agreement between measurement and calculations.

By the late 1970's coarse mesh 3-D neutronics calculations were assuming a major role in fuel management and core follow of reload cores. This occurred because of the degree of spatial inseparability of the neutron flux within reload cores. It was found necessary to account for these 3-D effects in the design and follow of each succeeding cycle. The ROCS code, which had been developed to provide such solutions while maintaining a realistic balance between speed and accuracy, was originally a modified one-group (1 1/2 energy group) code.[12] For reload cores in order to gain acceptable accuracy it was necessary to extend the ROCS formalism to 2-groups. When this was done errors were reduced to less than half their original values.[13] This use of coarse mesh codes required techniques to produce accurate homogenized cross sections. The DIT code based on integral transport theory has been developed and provides both fine and coarse mesh cross sections.[14,15] In addition, it is necessary to have a

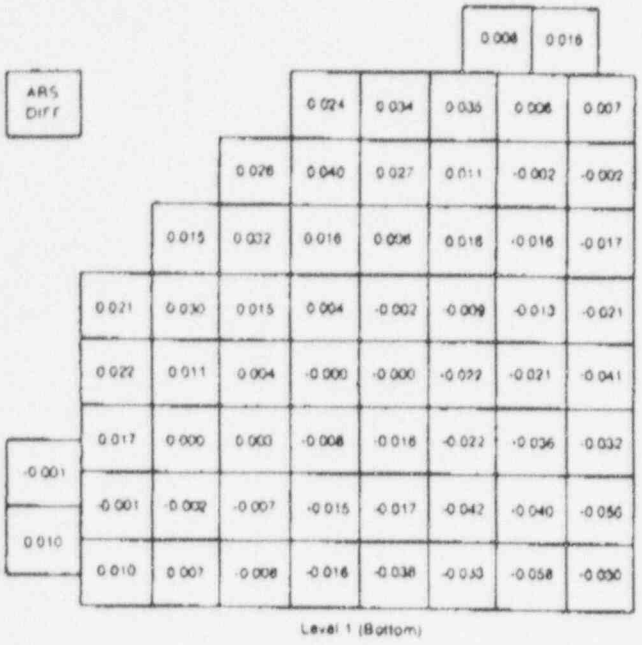

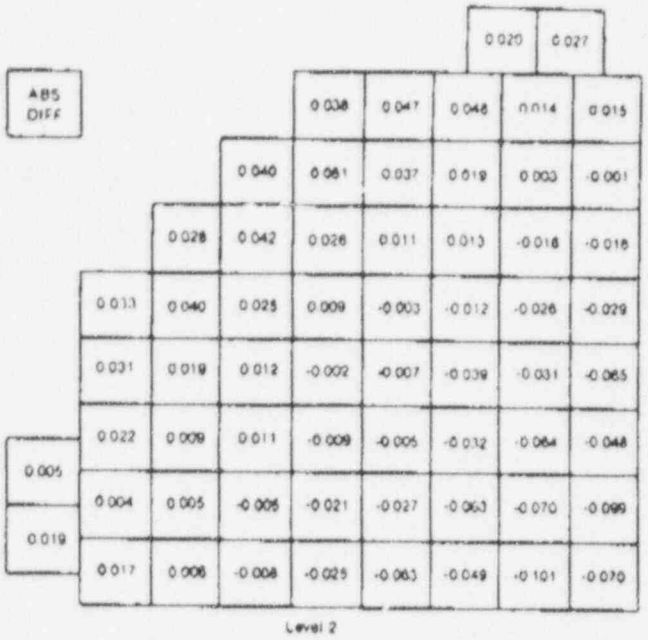

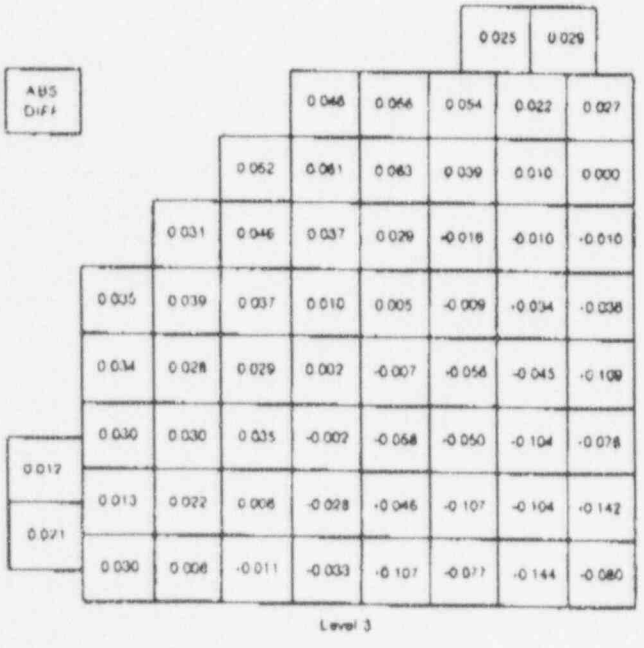

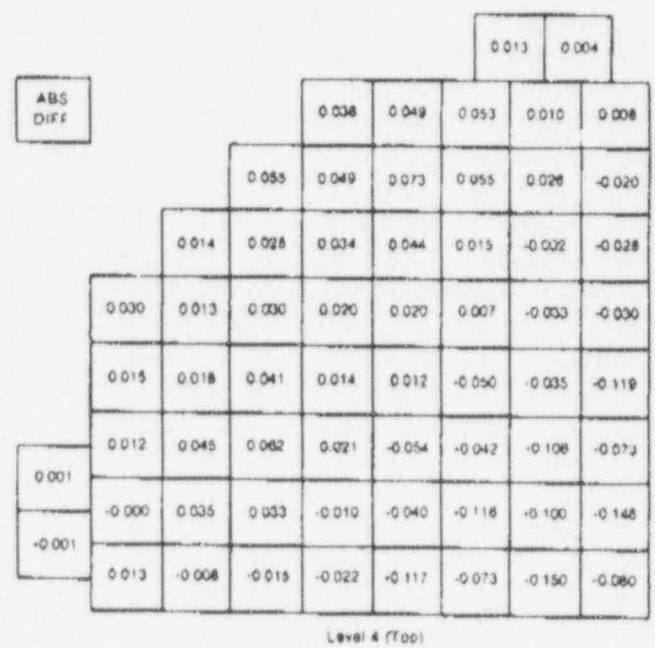

Fig. 18 Levelwise ROCS CECOR power comparisons showing effects of crud

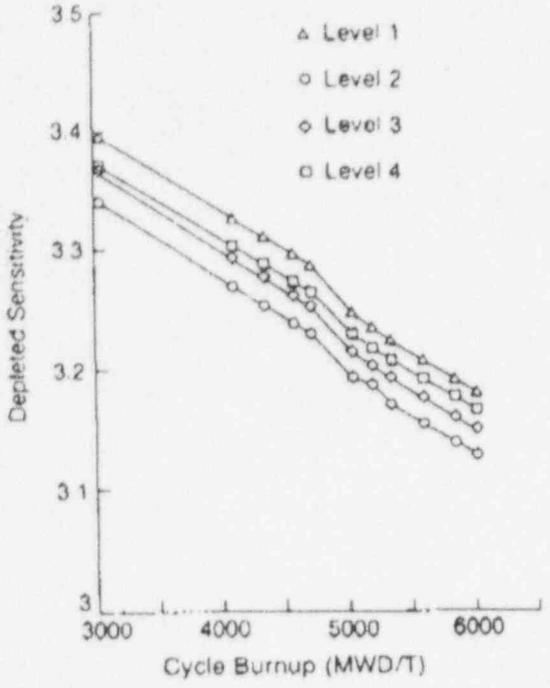

Fig. 19. Sensitivity depletion of typical instrument

method for obtaining local pin powers from coarse mesh results. This has led to the development of the MC program using the imbedded method for recovering local powers from core coarse mesh calculations.[20]

E. Verification of Detector Sensitivity Depletion Behavior

A more recent application has been to examine the detector sensitivity depletion behavior. The current produced by a self-powered rhodium detector is proportional to the product of the neutron absorptions in the rhodium and the beta escape probability neglecting the small fraction (1-2%) produced directly by gammas, i.e.

$$I = \varepsilon \bar{P} N_{Rh} \int_V \int_E \sigma \phi \, dE \, dV \qquad (14)$$

where

ε	is the electron charge
$\bar{P}$	is the average beta escape probability
σ	is the Rhodium cross section
ϕ	is the flux in the detector
N_{Rh}	is the average Rhodium number density
V	is the volume of the Rhodium emitter.

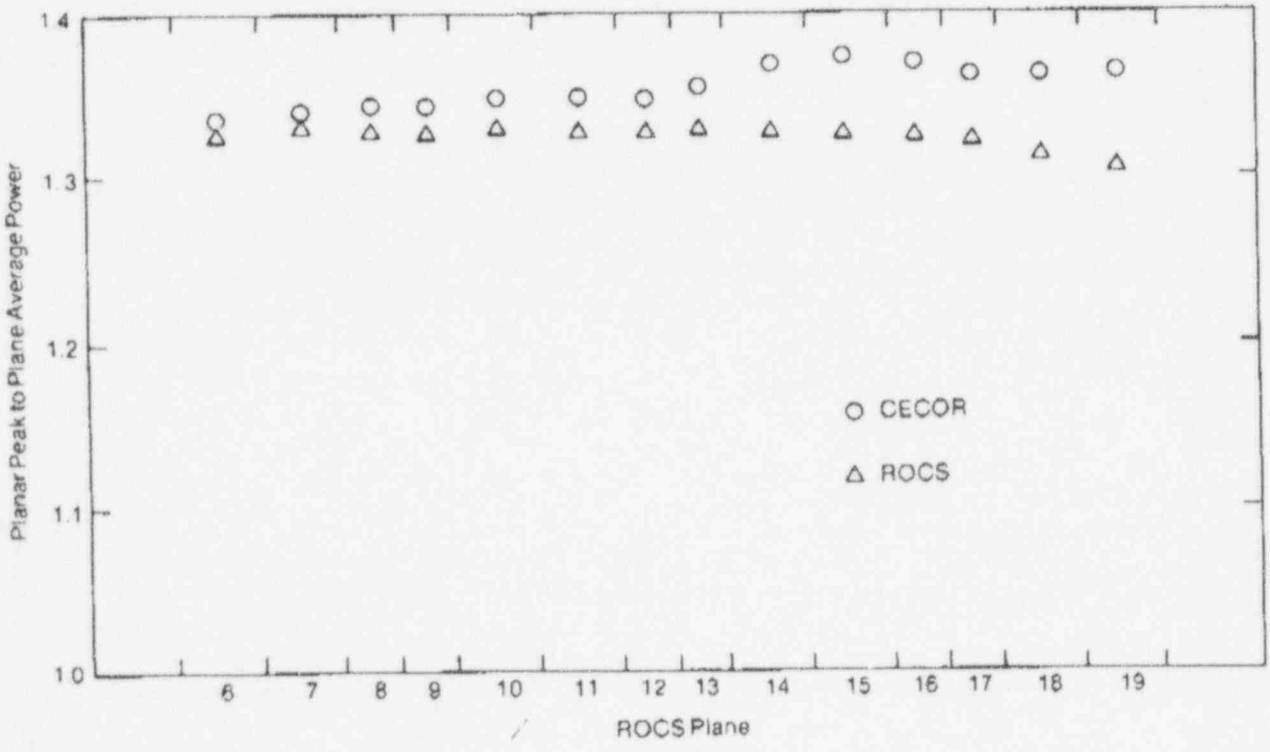

Fig. 20. Comparison of ROCS and CECOR planar peak to plane average box power (3-d multi-level coefficients)

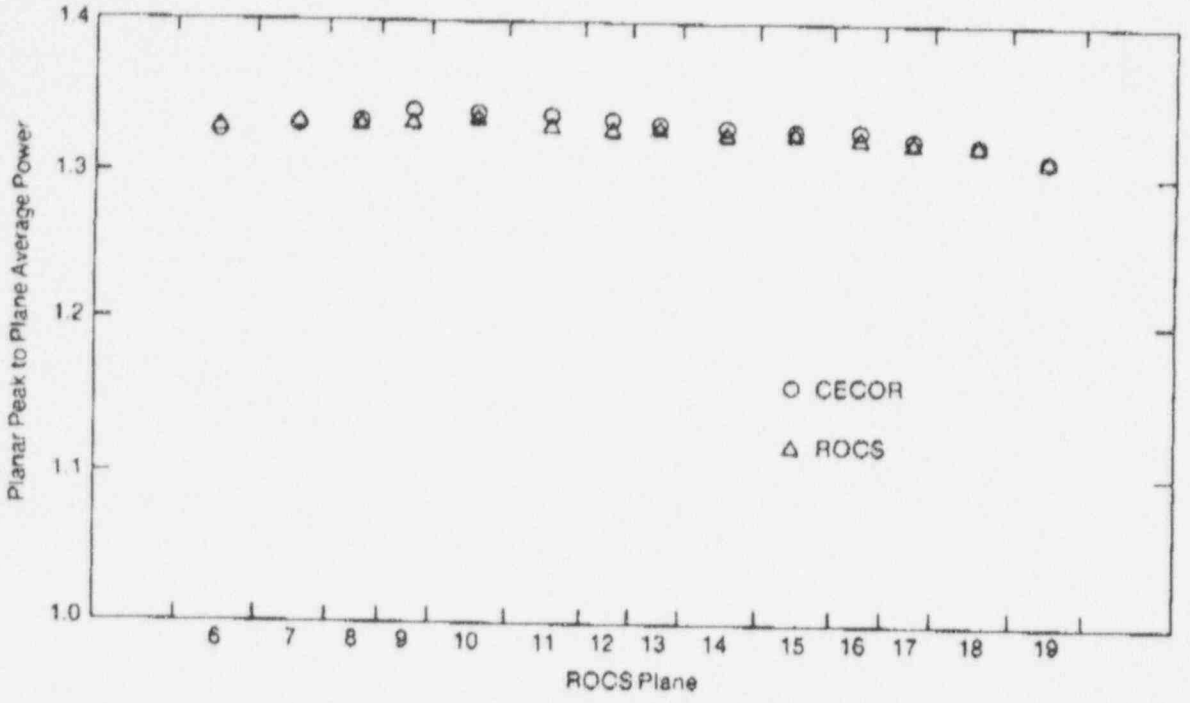

Fig. 21: Comparison of ROCS and CECOR planar peak to plane average box power (2-d single level coefficients)

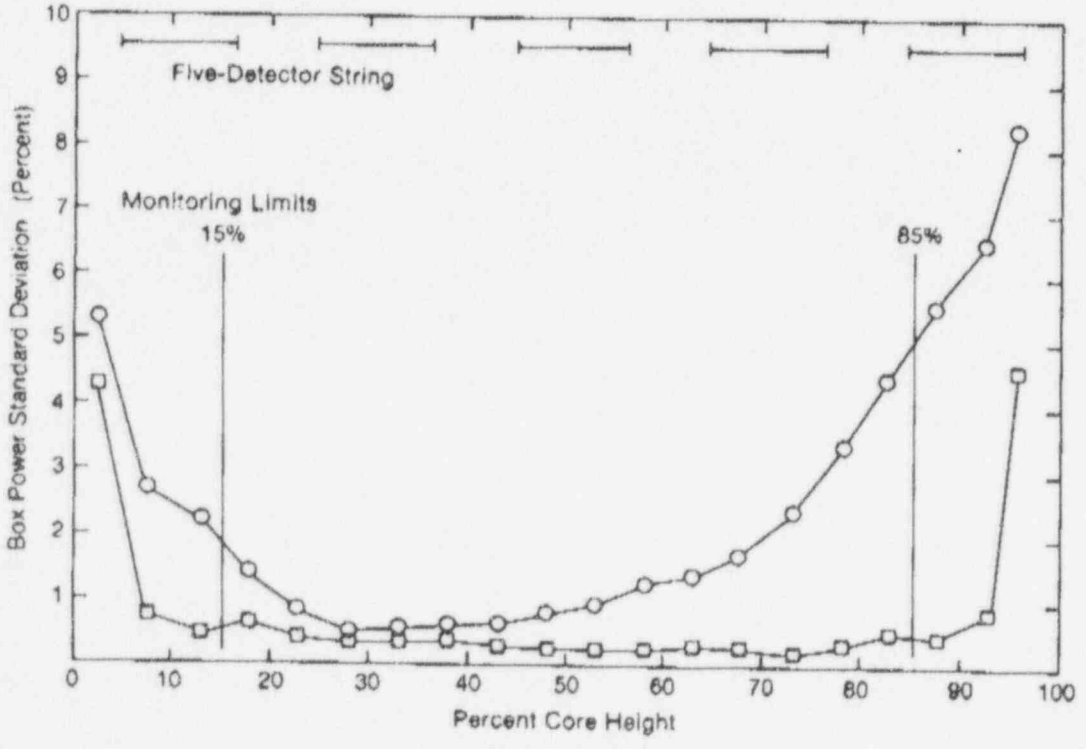

Fig. 22: Comparison of ROCS-CECOR planar box power synthesis errors using single- and multi-level coefficients (near BOC)

From Equation (14) the beta escape probability is determined as

$$\bar{P} = \frac{I}{\epsilon N_{\infty} \int_{V}\int_{E} \sigma \phi dE\, dV} \qquad (15)$$

If the detector sensitivity is based on currrent per rhodium activation, i.e.

$$S_{\infty} = \frac{I}{\epsilon \int_{V}\int_{E} \sigma \phi\, dE\, dV} \qquad (16)$$

it can be shown that the sensitivity follows a linear depletion law if the beta escape probability is constant with depletion

$$\frac{S}{S_o} = \left(1 - \frac{Q}{Q_{\infty}}\right) \qquad (17)$$

where

So	is the initial sensitivity
Q	is the accumulated charge
Q_{∞}	$= \epsilon \bar{P} V N_0$ is the theoretical total charge

Further, if the beta escape probability is constant with depletion, the accumulated charge also follows a linear law

$$Q = \epsilon \bar{P}\, V\, N_o \left(1 - \frac{N}{N_o}\right) \qquad (18)$$

where the slope is proportional to $\bar{P}$.

Currently, C-E and others employing fixed rhodium incores use a linear depletion law.[21] An initial study has been performed at C-E to evaluate this using operating data. Measured currents were compared to the rhodium activations and reaction rates calculated by the standard C-E coarse mesh ROCS code coupled with the newly developed and verified imbedded fine mesh assembly MC program.[20]. The calculations were carried out in a core-follow mode over the first three cycles of a typical C-E 2800 MW design in which detectors were depleted to about two-thirds of their theoretical charge.

Figure 23 shows the results of the sensitivity calculation. There is quite a bit of scatter but the entire ensemble demonstrates a linear depletion law with Q_{∞} of 308 coulombs. The scatter is caused to a large degree by the difference in the box power calculated by the ROCS core-follow models from that observed by CECOR. When the ROCS-MC activations are adjusted for these power differences, the scatter decreases greatly but cycle dependencies appear. This is shown in Figure 24. The resulting Q_{∞} is essentially the same with a value of 316 coulombs.

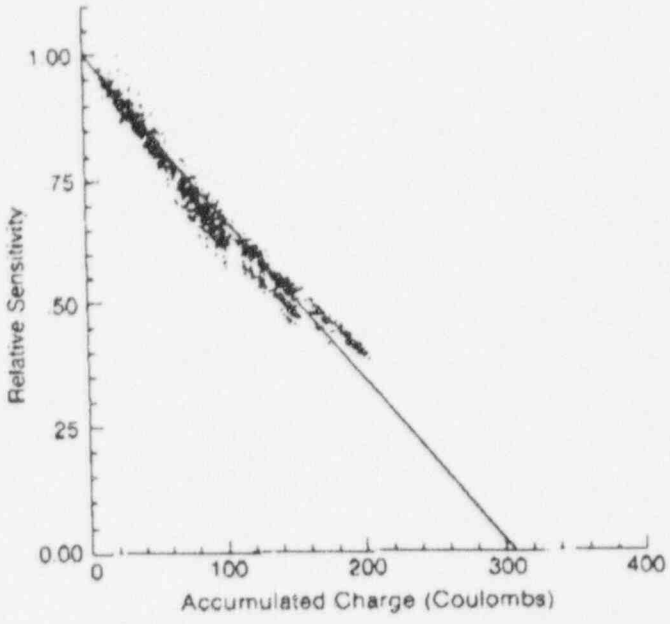

Fig. 23: Relative sensitivity

The linear behavior is not surprising since the beta escape probability was found to be essentially constant or flat over the cycle length. A typical example is shown in Figure 25 for an instrument that remained for the entire 3 cycles. The scatter during a cycle is on the order of 1-2%. There were also variations between cycles for

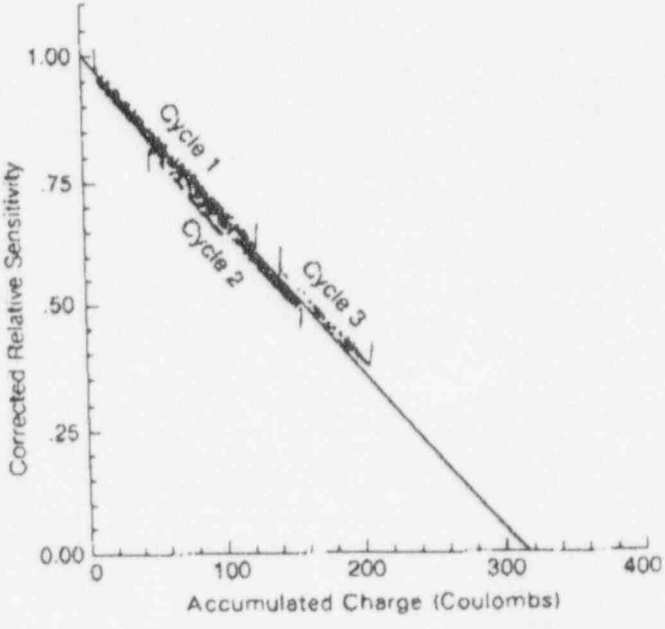

Fig. 24: Corrected Relative Sensitivity

any instrument on the order of 1-2%. These are apparently caused by modeling effects rather than actual physical effects. When the values are not adjusted for the differences between ROCS and CECOR box powers the scatter was larger, but the basic behavior was the same. The average value of the beta escape probability was about 0.40-0.42. This is consistent with values reported in the literature[22] for this diameter instrument.

The comparison of calculated rhodium number density for each cycle and accumulated charge is shown in Figure 26. The behavior is piece-wise linear with the intercept showing a Q_∞ of about 308 coulombs. The slope implies a beta escape probability of .403, consistent with the above observations.

This study tends to confirm the use of linear depletion law at least to about two-thirds depletion. Further work with more depleted instruments is necessary to confirm the law for higher depletions.

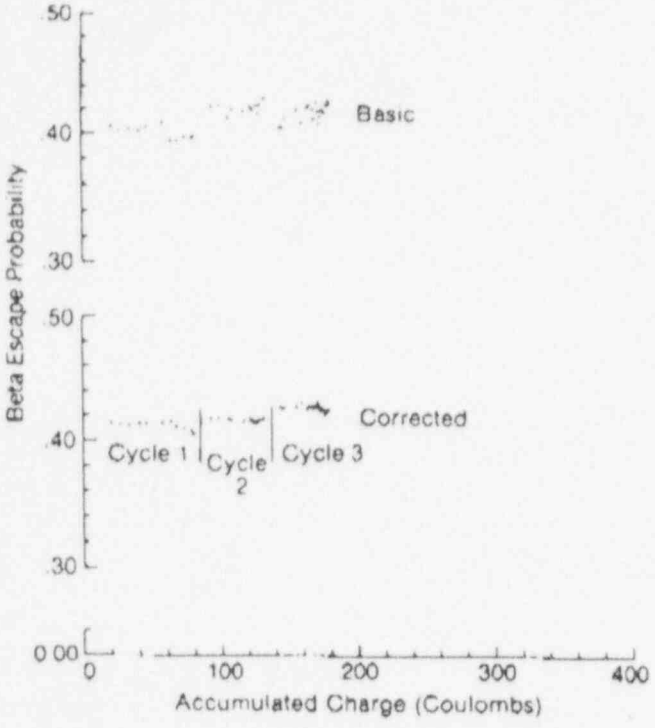

Fig. 25: Beta escape probability for a typical instrument

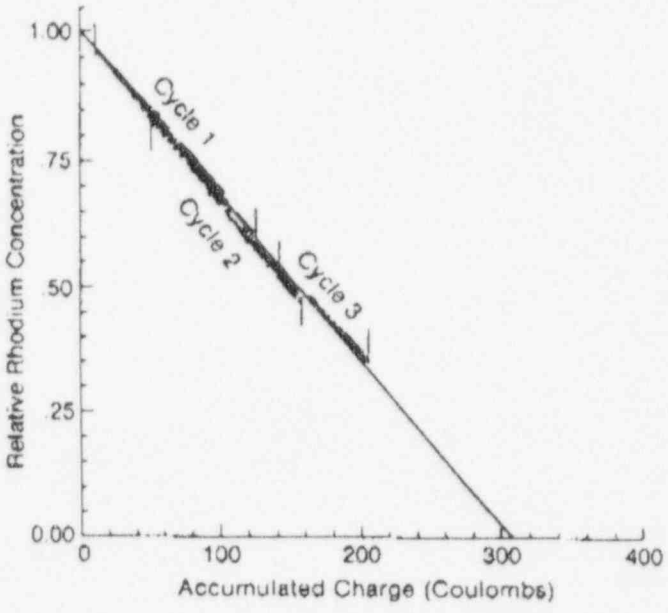

Fig. 26: Rhodium depletion

REFERENCES

1. R. I. Hellens, T. G. Ober, R. D. Ober, "A Method of Analyzing In-Core Detector Data in Power Reactors," Trans ANS, 12, 820 (1969).

2. T. G. Ober, P. H. Gavin, "Use of In-Core Instrumentation in Combustion Engineering Power Reactors," Trans ANS, 19, 218 (1974).

3. W. B. Terney, G. H. Marks, E. A. Williamson, Jr. and T. G. Ober, "Axial Power Distribution from Fourier Fitting of Fixed In-Core Detector Powers," Trans ANS, 22, 683 (1975).

4. W. B. Terney, T. G. Ober, and E. A. Williamson, Jr. "Three Dimensional Calculational Verification of C-E's In-Core Instrumentation System with Lifetime," Trans ANS, 22, 683 (1975).

5. W. B. Terney, E. A. Williamson, Jr. and T. G. Ober, "Calculation Verification of the Combustion Engineering Full Core Instrumentation Analysis System CECOR," Trans ANS, 24, 429 (1976).

6. A. Jonsson, W. B. Terney, M. W. Crump, "Evaluation of Uncertainty in the Nuclear Power Peaking Measured by the Self-Powered Fixed In-Core Detector System," CENPD-153-Rev. 1A, Combustion Engineering, Inc. (1980).

7. R. W. Knapp, C. R. Musick, "Digital Core Monitoring and Protection Systems," presented at IAEA Working Group on Nuclear Power Plant Control and Instrumentation, Specialists' Meeting, Cadarache, France, January 26-27, 1977 (C-E TIS-5111).

8. L. A. Banda, B. I. Nappi, "Dynamic Compensation of Rhodium Self-Powered Neutron Detectors," IEEE Transactions on Nuclear Science, Vol. NS-23, 1975, Pg. 311.

9. L. A. Banda, "Operational Experience in Rhodium Self-Powered Detectors," IEEE Transaction on Nuclear Science, Vol. NS-26, February 1979, Pg. 910.

10. A. Ralston, "A First Course in Numerical Analysis," McGraw Hill Book Co., 1967.

11. W. R. Caldwell, "PDQ-7 Reference Manual," WAPD-TM-678, January, 1969.

12. T. G. Ober, J. C. Stork, I. C. Rickard, J. K. Gasper, "Theory, Capabilities, and Use of the Three-Dimensional Reactor Operation and Control Simulator (ROCS)," Nucl. Sci. and Eng, 64 (605), 1977.

13. T. G. Ober, J. C. Stork, R. P. Bandera, W. B. Terney, "Extension of the ROCS Coarse Mesh Physics Simulator to Two Energy Groups," Trans. Am. Nucl. Soc., 28 (763), 1978.

14. A. Jonsson, et. al., "Discrete Integral Transport Theory Extended to the Case with Surface Sources," Atomkernenergie, Bd. 24, 1974.

15. A. Jonsson, et. al., "Verification of a Fuel Assembly Spectrum Code Based on Integral Transport Theory," Trans. Am. Nucl. Soc., 28 (778), 1978.

16. Combustion Engineering Standard Safety Analysis Report (CESSAR), Chapter 4.3.

17. Y. D. Harker, et. al., "Reactivity Measurements of St. Lucie Shims at the Advanced Reactivity Measurement Facility," Trans Am. Nucl. Soc. 26, (Supplement 1), 25 (1977)

18. W. B. Terney, "Albedo Adjusted Reflector Fast Diffusion Coefficient," Trans. Am. Nucl. Soc., 18, 319 (1974).

19. I. C. Rickard, N. R. Gomm, T. G. Ober, "Calculational and Experimental Verification of the Combustion Engineering Coarse Mesh Physics Simulator," Trans. Am. Nucl. Soc., 24, 340 (1976).

20. S. F. Grill, A. Jonsson, J. R. Rec, "A Nodal Imbedded Method to Recover Local Power Peaking from Coarse Mesh Reactor Calculations," Trans. Am. Nucl. Soc., 35, 580 (1980).

21. "Rhodium In-Core Detector Sensitivity Depletion," Interim Report NP-1405, EPRI, Palo Alto, California (May 1980).

22. T. Laaksonen, J. Saastamoinen, "Calculational Studies of Sensitivity Characteristics and Their Burnup Behavior for Rhodium Self-Powered Neutron Detectors," Proceeding of the IAEA Specialists Meeting on In-Core Instrumentation and Failed Fuel Detection and Location, AECL 5124, 111 (May 1974).

LIC-96-0108
Attachment 2

ABB

June 17, 1996
FC-PE-0057 Rev. 1

Ms. Jan Bostelman
Omaha Public Power District
P.O. Box 399
Ft. Calhoun, NE 68023-0399

Subject: **Fort Calhoun Cycle 16 Excore LHR LCO Reanalysis to Support Plant Operation Above 90% Power**

Dear Ms. Bostelman:

ABB has completed the reanalysis of Fort Calhoun Cycle 16 excore LHR LCO to support plant operation above 90% power. The purpose of the reanalysis was to determine an acceptable technical approach for operating the plant above 90% power until the completion of Cycle 16 in the event that the incore detector monitoring system is declared inoperable. This letter transmits the results of the reanalysis, which employed ABB's current setpoint analysis process for a variable (power level dependent) calorimetric power measurement uncertainty. In summary, operation at 100% power is allowed in the ASI range of -0.12 to +0.05 asiu provided the core is unrodded above 90% power. This result is applicable to Cycle 16 only. The details of the analysis are provided in the Attachment. The recommended approach does not change the results of the safety analysis or other setpoints for Cycle 16. The recorded calculation will be transmitted separately. The LHR LCO reanalysis was quality assured per the ABB CENO Quality Assurance Program.

If you have any questions, please call me at (860) 285-5512.

Sincerely,

COMBUSTION ENGINEERING, INC.

D. Bollacasa
Supervisor, Setpoint Analysis

ABB Combustion Engineering Nuclear Operations

Combustion Engineering, Inc. P.O. Box 500 1000 Prospect Hill Road Windsor, Connecticut 06095-0500 Telephone (860) 688-1911 Fax (860) 285-9512

Distribution:

M. J. Guinn	OPPD	
R. Jaworski	OPPD	(w/o Attachment)
R. C. Whipple	ABB	(w/o Attachment)
R. O. Doney	ABB	(w/o Attachment)
J. A. Noyes	ABB	(w/o Attachment)
R. T. Pearce	ABB	(w/o Attachment)
R. S. Spies	ABB	(w/o Attachment)

QR(2)

Attachment to FC-FE-0057 Rev. 1

Fort Calhoun Cycle 16 Excore LHR LCO Reanalysis

Purpose of Analysis

OPPD has been experiencing a high rate of incore detector failures during the operation of Ft. Calhoun Cycle 16. If the observed failure rate continues, the incore detector monitoring system may have to be declared inoperable before the end of Cycle 16. If this situation arises, Ft. Calhoun's procedures will allow the plant to continue to operate provided that the LHR and DNB LCOs are monitored using the excore detector monitoring system. However, the plant will not be allowed to operate at full power because the maximum power level permitted by the excore LHR LCO tent is presently 90% power. The excore DNB LCO tent supports full power operation.

The excore LHR LCO was reanalyzed for Ft. Calhoun Cycle 16 to justify operation at a power level greater than 90% until the end of Cycle 16 if the incore detectors are declared inoperable. This was accomplished by trading off LHR margin with imposed restrictions on plant operation above 90% power.

Analysis Summary

SCU penalty factors were calculated for use in the CESMAP runs based on the input uncertainties transmitted by OPPD in References 1 and 2. The CESMAP LHR LCO codes for the variable power measurement uncertainty process were utilized to calculate a new LHR LCO tent boundary and its corresponding N factor versus F_{xy}^{T} tradeoff curve. The physics, fuel performance, and transient analysis inputs for the CESMAP runs were based on the numerical data in the INPUT3.LCO electronic file transmitted to ABB through Reference 1 and confirmed in Reference 2.

The CESMAP LHR LCO analysis took credit for plant operation in an unrodded configuration for power levels above 90%. An unrodded configuration has been defined as a configuration which allows for exercising of the CEAs, but not allowing insertion for prolonged periods of time beyond the 126 inches withdrawn position. An improvement in the maximum allowed power level was accomplished by restricting increased radial peaking at high power levels by requiring that the lead bank be fully withdrawn. ABB's analysis supports the excore LHR LCO tent shown in Figure 1 and the N factor versus F_{xy}^{T} tradeoff curve shown in Figure 2 for Cycle 16 with the following operating limitations, which must be implemented administratively in the event that the LHR LCO has to be monitored with the ex-core system, such as when the incore detector system is declared inoperable:

1. The reactor core must be completely unrodded before the power level is allowed to increase above 90% power.

2. The CEAs cannot be inserted while the power level is greater than 90% power and any power reduction must be accomplished through changes in the soluble boron concentration or some other reactivity adjustment. Otherwise, the reactor power level must be reduced to a value less than or equal to 90%.

3. CEA insertion is permitted up to the PDIL Long Term Insertion Limit (25% insertion of CEA group 4) when the power level is less than or equal to 90%.

It should be noted that the N factor versus F_{xy}^T tradeoff curve is intended for situations where the incore detector system can still be utilized (directly or indirectly) to measure F_{xy}^T. If the incore detectors are declared inoperable, it would be prudent to monitor with the excore LHR LCO tent provided that the predicted maximum unrodded F_{xy}^T for the remaining part of the core Cycle (including appropriate calculative uncertainties) does not exceed the COLR limit of 1.86. This situation is equivalent to having an N factor of unity (i.e., 100%) for the remaining part of the core cycle as show in Figure 2.

The recommended changes to the excore LHR LCO tent and the N factor versus F_{xy}^T tradeoff curve does not change the results of the safety analysis or other setpoints for Cycle 16.

ABB recommends that the following note be added to the COLR Figure for the LHR LCO tent as in Figure 1:

"Note: Rodded operation is not allowed above 90% of Rated Thermal Power."

References

1. Letter, J. L. Bostelman (OPPD) to D. Bollacasa (ABB), "Data Transmittal for Support of ASI Tent Expansion at Low Powers," PED-DEN-96-0268, May 6, 1996.

2. Letter, J. L. Bostelman (OPPD) to D. Bollacasa (ABB), "Confirmation of Uncertainties for the LHR LCO Tent Reanalysis," PED-DEN-96-0306, June 4, 1996.

Figure 1

Fort Calhoun Cycle 16 Ex-Core LHP LCO Tent

(Note: Bodded operation is prohibited above 90% of Rated Thermal Power.)

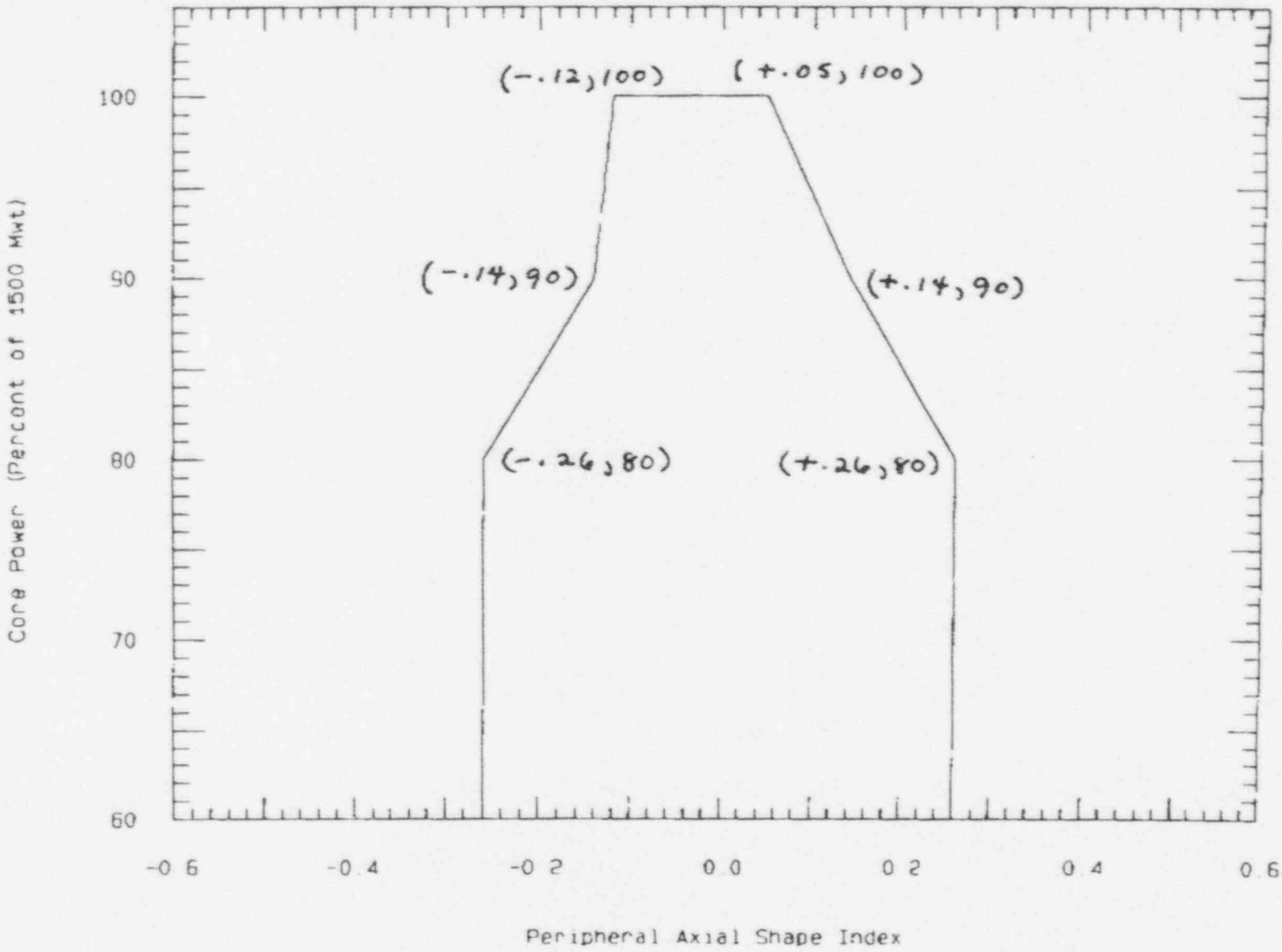

Figure 2

Fort Calhoun Cycle 16 N Factor Curve

(Note: Rodded operation is prohibited above 90% of Rated Thermal Power.)

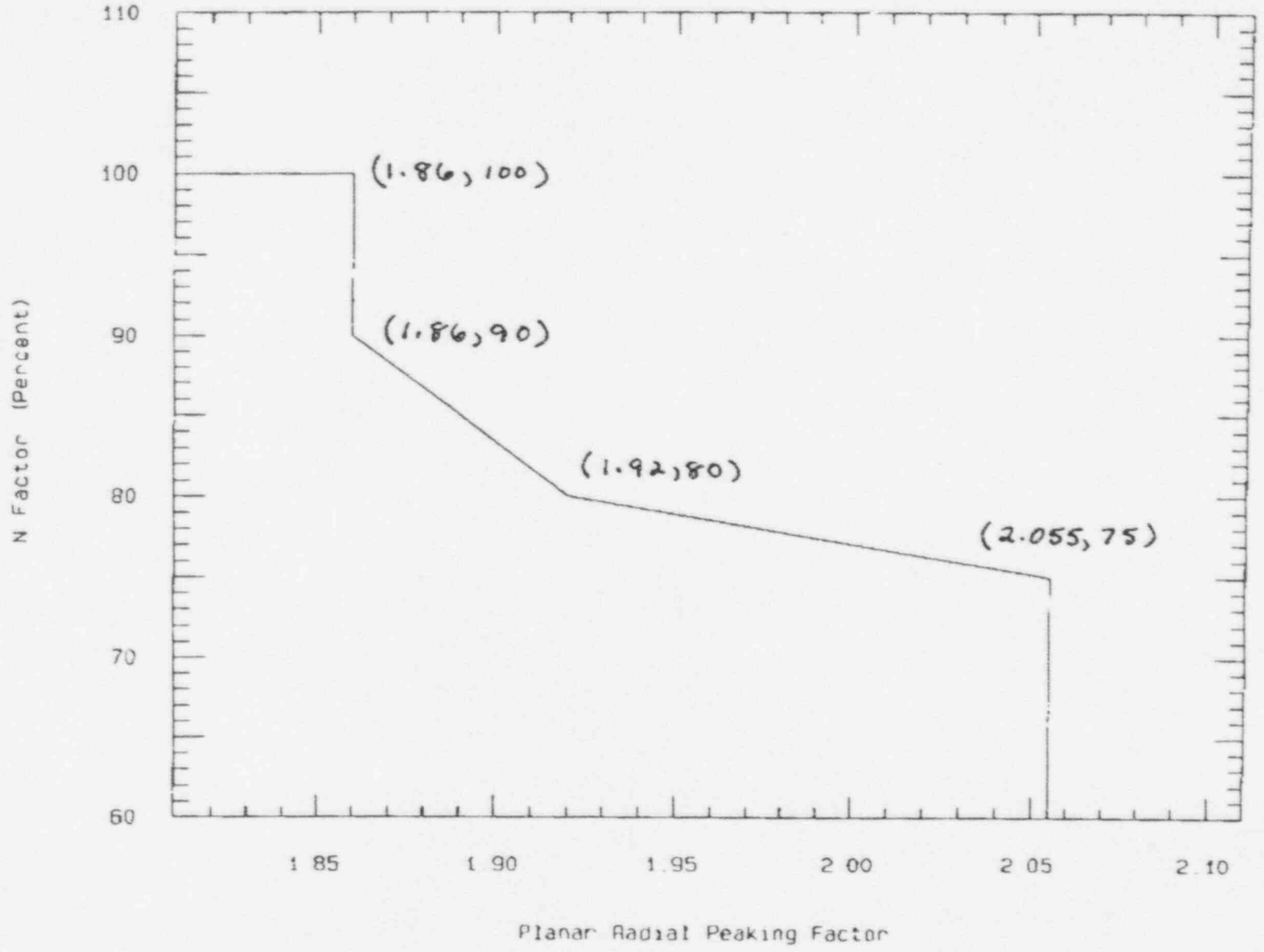

EXECUTIVE SUMMARY

ISTC TECHNICAL PROCESS REVIEW

(Fort Calhoun First-Cycle ICI Failures)

June 3-7, 1996

Team:
R. Driscoll (ABB)
P. Hellandbrand (ABB)
C. Hoffmann (ABB)
P. Kasik (MPR Associates)
K. Margotta (ABB)
D. Sylvain (ABB)

ABB CE NUCLEAR OPERATIONS

June 19, 1996

NOTICE

The information, assessments and conclusions set forth herein are preliminary, and should not be used or construed as final. The root cause analysis review is ongoing, and the content hereof is subject to further review and revision.

1.0 EXECUTIVE SUMMARY

As a result of the recent increase in In-Core Instrument (ICI) field failures, particularly first-cycle failures at Fort Calhoun (OPPD), ABB CENO performed a Technical Process Review at the ICI manufacturer, Image and Sensing Technology, Canada (ISTC). This review was part of a Root Cause Analysis (RCA) being performed by ABB to investigate not only potential causal factors related to ICI Materials and Manufacturing, but also all other potential causal factors in the areas of Core Operations, Maintenance, and ICI Installation. The RCA is being pursued in parallel with the Materials and Manufacturing investigation, and a final RCA report will be issued upon its completion (targeted for late summer, 1996).

This report summarizes the results of the ISTC Technical Process Review. It was performed during the week of June 3-7, 1996 by a team of five ABB personnel and one consultant from MPR Associates (based in Alexandria, Virginia). The objective was to collect data for the sole purpose of identifying materials and manufacturing - related potential causes of the OPPD first-cycle ICI failures. The approach was a technically-oriented review and involved observing work in process, evaluating hardware, talking with operators, and reviewing actual product records including material certifications, inspection reports, radiographs, photomicrographs and metallographic mounts.

Although the failure mechanism has not yet been confirmed by examination of a failed ICI, field failure data from Ft. Calhoun indicates the most probable failure mechanism to be a breach of the individual detector sheath, allowing moisture to get into the instrument and cause a short circuit. A preliminary review of available information suggests that stress corrosion cracking (SCC) may be a contributing factor in causing the breach. Correlation of failures with manufacturing information indicates that certain manufacturing batches have a higher frequency of first-cycle failures. This information was used to focus the technical process review on certain key areas:

- ICI's manufactured for Fort Calhoun in particular. Although information was collected that will assist in evaluating failures at other plants, the primary focus was on those instruments experiencing high first-cycle failures at Fort Calhoun.

- The individual detector material procurement and fabrication process, rather than the entire instrument fabrication process.

- Three specific production time periods, as represented by certain batches of detectors. These periods represented "normal field performance", "high first-cycle failure field performance", and "current detector production"; i.e., those detectors fabricated but not yet assembled into instruments.

1.0 EXECUTIVE SUMMARY (Continued)

- Changes between, and problems during, each of these three production time periods. This was based on the premise that something has changed, since the high frequency of first cycle failures is a recent phenomenon (starting in Cycle 16 at Fort Calhoun).

- The areas of ISTC design, materials, fabrication, and inspection (results and trends). These areas would cover the full range of materials and manufacturing activities.

This review identified a total of twelve changes that occurred between the "normal field performance" production period and the "high first cycle failure" production period. One of these changes is believed to be significant relative to increasing the susceptibility of detectors to stress corrosion cracking. A change was made in the detector tubing starting material (Inconel 600) which, beginning around 1990, included a nominal 10% cold work as opposed to the previous fully annealed condition. This was done to eliminate problems being encountered with the fully annealed tubing during manufacturing (e.g., kinking during loading of insulators). Review of mechanical properties data from materials certification reports indicates that the initial cold work levels in the starting material could be up to 25%.

This change and the variability of the starting material in the cold worked condition is reflected in a variation in the grain structure. The microstructure of some detector tubing exhibits relatively uniform grain size through the detector wall. Grain size is estimated to be ASTM ~ 7-8. Microstructures of the other batches of detectors exhibit a much finer grain size, typically ASTM 10, with considerable variation of the grain size through the wall thickness of the detector. In general, larger grains were observed on the outside diameter surface with increasingly finer grains near the inside surface. The net effect of this is that there is a noticeable variation in the final microstructures between batches of detectors. The variations in microstructure may result in some material being more susceptible to stress corrosion cracking than others. At this time, the magnitude of this increase in susceptibility is not known.

1.0 EXECUTIVE SUMMARY (Continued)

One other change was noted in the context of increased susceptibility to stress corrosion cracking. This change was a reduction in the final annealing temperature from ~ 1900°F to ~ 1650°F, which occurred around 1981-82, prior to all three of the "specific" time periods covered during the review. Heat treatment of Inconel 600 at a temperature of 1650°F does not produce a complete anneal of the material. This temperature is high enough to produce recrystallization in the cold worked material but too low to solutionize the carbides present in the material. As a result, when recrystallization occurs, the resultant location of the carbides is intragranular. The heat treatment results in a fine grain structure, with few carbides on the grain boundaries, some residual cold work, and moderate to high strength. All three of these conditions are considered to make Inconel 600 tubing more susceptible to stress corrosion cracking when exposed to PWR environments.

As noted above, a comparison was also made between the "high first cycle failure" production period and "current detector" production period. Only three changes were noted and none of them are considered significant relative to increasing material susceptibility to SCC.

Based on the above, the preliminary findings of the Root Cause Analysis can be summarized as follows:

There may be an increased susceptibility to SCC in the material used to manufacture the ICI's that experienced first-cycle failures at Fort Calhoun. Similar material may also be present in other ICI's installed at other CE plants (i.e., Calvert Cliffs 1 and 2; St. Lucie 1 and 2; and Millstone 2)[1]. The magnitude of this increase is unknown at this time. It is unclear, at this time, whether these conditions by themselves, or in combination with currently unknown factors, are sufficient to cause the failures at Fort Calhoun, and other CE Plants that recently began experiencing high failures rates. It is conceivable that multiple causal factors are involved in these failures (i.e., increased material susceptibility to SCC along with a more severe temperature and/or stress environment and/or instrument and maintenance handling issues). If this is true, failures may occur more readily at some plants than at others. ABB CENO is continuing its investigation in an attempt to more completely identify and assess these potential causal factors. The results will be reported in the final root cause analysis report, targeted for completion late this summer.

---

[1] Note that the failures at other CE plants have occurred more frequently in the 2nd and 3rd cycles, not the first cycle as has occurred at Fort Calhoun